ELECTRONIC AND ELECTROMECHANICAL TESTER

FOR PHYSIOLOGICAL SENSORS

by

JOHN BRYANT GRACE JR.

TIMOTHY A. HASKEW, COMMITTEE CHAIR
EDWARD S. SAZONOV
KENNETH G. RICKS
KEITH A. WILLIAMS

A THESIS

Submitted in partial fulfillment of the requirements
for the degree of Master of Science
in the Department of Electrical and Computer Engineering
in the Graduate School of
The University of Alabama

TUSCALOOSA, ALABAMA

2013

ABSTRACT

Historically, physiological sensors used for measuring respiratory, cardiovascular and electrodermal activity have been used with polygraph devices and sleep laboratories. Periodic testing of these sensors is imperative to maintain sound performance of the measurement device. This thesis presents an Electronic and Electromechanical Tester (EET) for physiological sensors used with polygraph instruments that can accurately and repeatedly reproduce both physiological signals originating from the human body as well as computer-generated signals. The tester is interfaced to a personal computer via USB and contains the following four time-synchronous channels: two electromechanical simulators for testing abdominal and thoracic respiratory sensors, an electromechanical simulator for testing a sphygmomanometer used to capture cardiovascular activity, and an electronic simulator for testing electrodermal sensors. All of the simulated physiological channels apply direct physical actuation to the corresponding sensors.

Specifics of software architecture and hardware implementation are included along with validation examples and test results. System identification techniques are discussed and transfer function models are defined. Based on these transfer function models, a compensator is designed with a goal of improving validation test data. The EET demonstrated its ability to reproduce physiological signals with adequate accuracy and repeatability. Finally, future systematic improvements as well as additional application areas are explored.

LIST OF ABBREVIATIONS AND SYMBOLS

AC	Alternating current
a_c	Acceleration profile for cardiovascular channel
ADC	Analog to digital converter
a_r	Acceleration profile for respiratory channel
cm	Centimeter
CRC	Cyclic Redundancy Check
DACA_ASCII	Standard output file format for polygraph examinations
DC	Direct current
EDA	Electrodermal activity
EEPROM	Electrically erasable programmable read-only memory
EET	Electronic and Electromechanical Tester
EKG	Electrocardiogram
E_{MEAN}	Mean absolute difference between test signals and mean signal
E_{REF}	Mean absolute difference between test signals and reference signal
F	Force
f_c	Maximum actuation frequency for cardiovascular channel
FIFO	First-in first-out; method for organizing a data buffer
f_r	Maximum actuation frequency for respiratory channel
G(s)	Continuous-time subsystem transfer function
$G_1(s)$	Transfer function defined as S/I

$G_2(s)$	Transfer function defined as P/S
$G_C(s)$	Subsystem compensator defined as $G(s)^{-1}$
$G_C(z)$	Discrete-time realization of $G_C(s)$
GSR	Galvanic skin response
GUI	Graphical User Interface
Hz	Hertz; unit of frequency
I	Used to describe the input signal to the system
I/O	Input/Output
l	Actuator screw lead for respiratory and cardiovascular channels
LTI	Linear time-invariant
m_c	Actuator carriage mass
mm	Millimeter
mmHg	Millimeters of mercury; unit of pressure
m(t)	Mean signal obtained from point-to-point average of all test signals
N-m	Newton-meter; unit of torque
OS	Operating system
P	Used to describe output signal captured by polygraph
PC	Personal computer
r(t)	Reference signal used in validation tests
S	Used to describe linear displacement of actuator carriage

SRAM	Static random-access memory
STD	Standard deviation
STD_{MEAN}	Average standard deviation of test signals relative to their mean
T	Torque
USB	Universal Serial Bus
v_c	Velocity profile of cardiovascular channel
v_r	Velocity profile of respiratory channel
x_c	Position profile of cardiovascular channel
x_r	Position profile of respiratory channel
x(t)	Test signals obtained from validation tests
ω_c	Maximum angular frequency for cardiovascular channel
ω_r	Maximum angular frequency for respiratory channel
Σ_N	Sigma notation; summation of terms from 1 to N

ACKNOWLEDGEMENTS

I would like to take this opportunity to thank my fellow students, friends and faculty members that have made the completion of this thesis a success. Firstly, I would like to thank Andrew Price and Nagaraj Hegde for their involvement in this research project. I would like to especially thank Dr. Haskew for all his support during the completion of this research project and thesis, and for providing me with guidance through my graduate studies. Many thanks to Dr. Sazonov for allowing me to be a part of this research project, as well as to my committee members Dr. Ricks and Dr. Williams for your valuable input into my research. The members of my committee have made contributions that have not only made this thesis possible, but have also inspired me in the progress of my research. I would like to thank Dr. Dollins for his support during this project, and for the many hours he spent in off-site testing and collecting data. Finally, I would like to thank my parents for their unconditional love and support through my academic progress.

CONTENTS

LIST OF TABLES

LIST OF FIGURES

CHAPTER 1

INTRODUCTION

Polygraph tests have been issued by law enforcement officials and security forces since the 1920s [1]. Currently, polygraph testimonies are admissible in court in 19 states in the United States of America and are actively used as an investigative tool in Canada [2]. Due to contentious debate and controversy surrounding the legitimacy of the scientific basis of psychophysiological detection of deception [3], polygraphs and polygraph evidence are less commonly used and typically not admissible in court in many other countries [4]. Even so, polygraphs are commonly used as a screening tool for hiring new employees into security-sensitive positions and national security matters.

The polygraph is a device that monitors several physiological indices (such as skin conductivity, respiratory activity, pulse and blood pressure) during an interview in which the subject is asked a series of predetermined questions. The polygraph records these physiological signals obtained through the corresponding sensors for later examination by a trained polygraph examiner. The expectation is that deceptive answers will register different physiological responses from those corresponding to truthful answers. The polygraph instrument, therefore, is not a device that detects deception. Rather, it is a recorder of physiological responses [5]. The first commercially available polygraphs consisted of pneumatically driven pens to record the emotional responses of the test subjects. The modern instruments are computerized and create digital recordings of physiological signals captured during an interview.

Skin conductivity (also called electrodermal response or Galvanic Skin Response, GSR) is thought to be an indicator of psychological, emotional or physiological arousal. Measurement of skin conductivity is typically performed by a digital ohmmeter in which a constant 0.5V is applied between the electrodes and the resulting current flow is measured by amplifying the voltage across a resistor in series with the skin [6].

Respiration in polygraph equipment is typically monitored using pneumatic pressure gauges. The process of breathing expands and contracts abdominal and thoracic gauges. This produces variations in air pressure within the gauge which are then captured by an air pressure sensor within the polygraph [5]. Piezoelectric or capacitive breathing sensors incorporated into elastic belts could also be used.

Cardiovascular activity such as heart rate and variation in blood pressure is normally examined by a sphygmomanometer (with the cuff typically inflated to 60mmHg). Blood pressure is the force exerted on the outside walls of blood vessels throughout the body as the heart contracts and relaxes. The pressurized cuff of the sphygmomanometer captures cuff-pressure oscillation [7]. A pressure transducer within the polygraph instrument captures and records this change in pressure.

Since polygraph testimony is still in wide use, it is essential to understand how different polygraph instruments respond to identical excitations. This will not only aide in correctly identifying physiological responses between various subjects, but will also validate and calibrate physiological sensors and thus ensure reliability of obtained readings. This thesis will present an Electronic and Electromechanical Tester (EET) designed to test physiological sensors typically used with polygraph instruments. The EET is capable of accurately and repeatedly reproducing previously recorded physiological signals originating from the human body as well as custom

computer-generated signals. In this sense, the EET provides a simulation of the real physiological processes and provides an accurate and repeatable way of testing polygraph equipment. Chapter 2 will cover the software architecture and implementation used in the EET. The software architecture of the EET can be broken down into two sections. The first section is the front-end PC GUI and the second section is the microcontroller firmware. Chapter 3 will cover the hardware specifications and implementation including all electrical and mechanical aspects of the simulator. Each subsystem will be broken down into detail. Chapter 4 demonstrates the validation and verification of the EET by presenting accuracy and repeatability tests and results. Chapter 5 provides system identification and transfer function modeling of the electromechanical channels of the EET. A compensator is then designed to reduce the absolute error produced by the EET. Chapter 6 reveals the implementation and results of the compensator that was introduced to the system. And finally, Chapter 7 provides a necessary conclusion to this thesis and presents possible future work and research opportunities.

CHAPTER 2

SOFTWARE ARCHITECTURE

It is necessary to first discuss the underlying software architecture of the EET that controls the actuation of each physiological channel. The software architecture of the EET can be broken down into a front-end graphical user interface and a back-end microcontroller firmware. Before delving into software details, a high level overview of the system architecture of the EET and the system requirements of the EET will be covered.

2.1 System Requirements

The requirements for the EET were constructed based on the fundamental physiological properties of respiration, galvanic skin response and cardiovascular activity. Such factors that were taken into consideration include physical actuation range and frequency of events. The system requirements cover the entire physiological actuation range that the typical human body is capable of producing. Table 1 lists the physiological signal sources (originating from human body), measurement sensors (on polygraph), actuation transducers (on EET) and desired ranges, rates and resolutions of the actuation.

Table 1. EET System Requirements

Physiological source	**Measurement sensor**	**Actuation transducer**	**Actuation resolution**	**Actuation range**	**Actuation rate**
Respiratory	Pneumatic pressure gauge	Screw-driven linear actuation	≥ 12 bits per full range of motion	0 – 5 cm	0 – 30 breaths per minute
Cardiovascular	Sphygmoman-ometer	Screw-driven linear actuation	≥ 12 bits per full range of motion	20 – 200 mmHg	40 – 200 beats per minute
Galvanic skin response	0.5V resistance measurement circuit	Switch-based resistive circuit	≥ 12 bits per full range of motion	1k Ω – 4.096 MΩ	0 (DC) – 60 Hz

2.2 EET System Architecture

A high-level diagram demonstrating the system architecture for the EET is shown in Figure 1. A personal computer (1) with the C# graphical user interface (GUI) desktop program reads the files containing recordings of physiological signals and sends them to the microcontroller (2) through a USB-to-serial converter on the Arduino Mega2560 [8] microcontroller board. This acts as the direct communication link between the personal computer running the C# desktop program and the EET. The interface to the EET is implemented as a virtual serial port connection through a USB port using the ATmega16U2 [9] on the Arduino Mega2560 programmed as a USB-to-serial converter. The ATmega16U2 chip supports bidirectional data exchange with rates up to 12 Mbit/s, which is more than sufficient for the application. With simultaneous playback of four channels at a sampling rate of 60 Hz and 16 bit resolution, the required data rate is below 4 kbit/s. The microcontroller buffers short periods of recordings in internal memory. The microcontroller also converts the waveform data points received from the personal computer into move commands issued to digital motor controllers (4) that drive linear actuators (5) for the electromechanical respiratory and cardiovascular channels.

The microcontroller also controls a switch-based resistive circuit (3) that simulates GSR. The microcontroller used in the design is an ATmega2560 [10] (on the Arduino Mega2560 board).

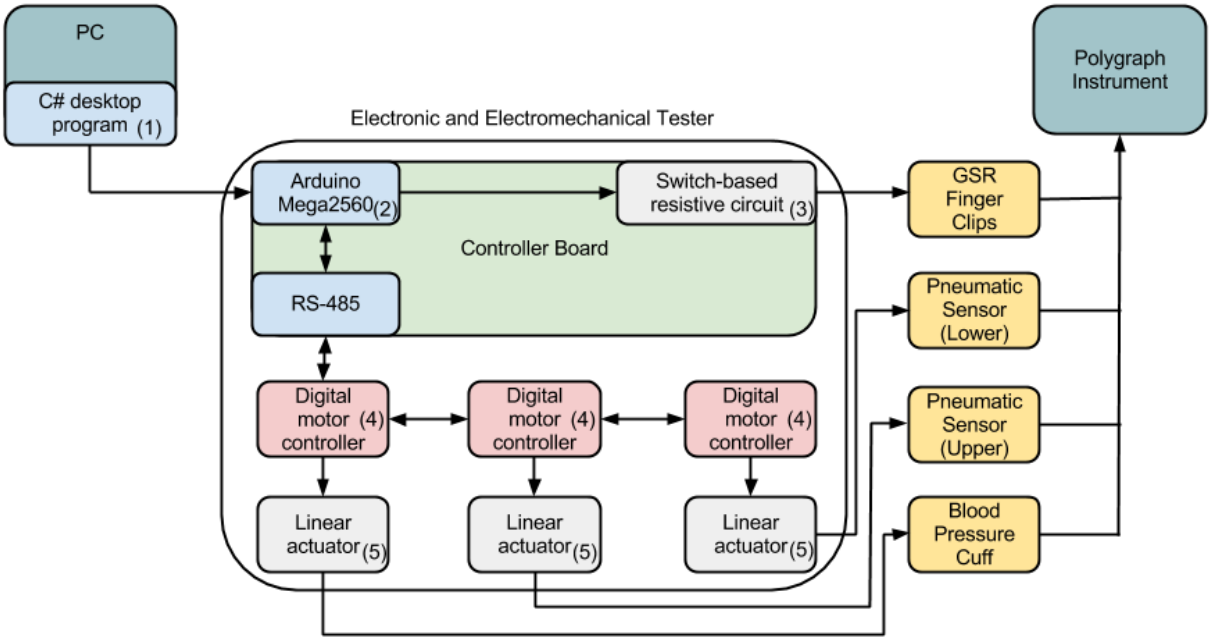

Figure 1. High-Level System Architecture Diagram of EET

2.2.1 Front End Graphical User Interface

The PC graphical user interface software allows the user to interface directly to and control the operation of the EET. Written in C# using Microsoft Visual Studio, the graphical user interface allows the user to browse to a DACA_ASCII file and load an image of the waveform onto the screen. This allows for visualization of the waveform currently being simulated by the EET. The GUI also has the capability to generate standard waveforms of varying frequency, amplitude and offset. These waveforms include a sinusoidal wave, square wave, triangular wave, data point sweep, and sinusoidal frequency sweep. This was implemented into the system to give the user the opportunity to test physiological sensors with a known periodic waveform. A

screenshot of the GUI is shown in Figure 2. This demonstrates what the GUI would typically look like during playback of a waveform.

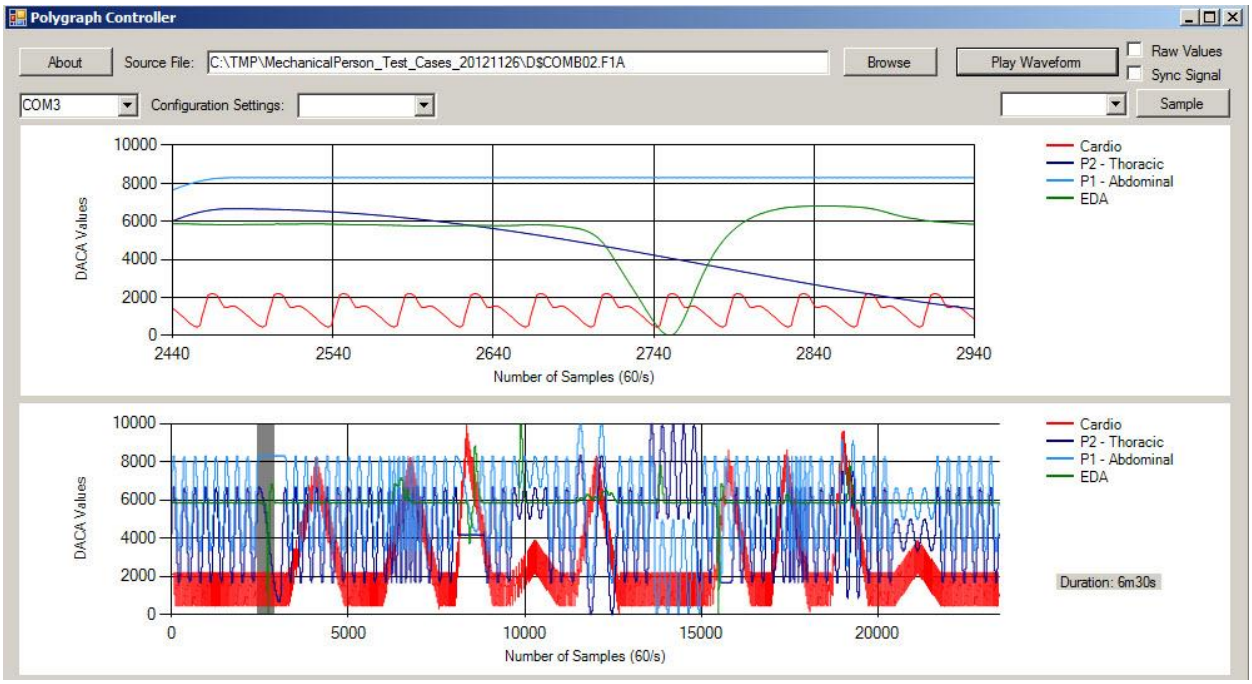

Figure 2. Screenshot of GUI

The DACA_ASCII file format is the standard file format for polygraph examiners to read polygraph tests. The data is scaled to a 0 – 10,000 DACA value range. Because of this scale, physiological actuation data included in a DACA_ASCII file is essentially unitless. More information on DACA_ASCII file formatting and unitless DACA values is provided in Chapter 4.

Upon execution of the program, the user will browse for a DACA_ASCII file containing physiological waveforms. When a DACA_ASCII file is successfully chosen, the GUI software will scan the file until it reaches the data section containing waveforms for each physiological channel. For each line of data from the DACA_ASCII file, a new sample is generated containing

four data points (one for each physiological channel represented on the EET). Then, a list is generated from each new sample that can be accessed by index. Once the list is successfully generated, samples in the list get added to a chart on the screen. Two charts are generated – one containing the entire waveform, and another scaled chart containing the previous 500 samples played. This will give the user a visual of the waveforms being reproduced on all four physiological channels. When the play button is pressed, a serial connection is opened and a data burst is populated. A data burst is a short recording of data that will be periodically sent to the microcontroller via the serial connection. Each data burst has a static size of 30 samples. The serial port is then continuously read until a status flag is received from the microcontroller. This indicates that the microcontroller is requesting more data. The data burst is then written to the serial port. Next, indices and chart positions are updated, and a new data burst gets populated. When the end of the chart has been reached, the EET will stop and wait for further instructions from the user.

For computer-generated signals, each data point list is created from user input. For example, the user can specify a sine wave of a known frequency, amplitude, offset and duration. A data point list is then generated from samples created by this information from the user. This gives the user the option of testing each physiological sensor with a custom periodic signal of known frequency, amplitude and duration.

2.2.2 Microcontroller Firmware

As previously mentioned, the microcontroller board used on the EET is an Arduino Mega 2560 featuring an ATmega2560 microcontroller. It includes 54 digital IO pins, 16 analog inputs with a 10 bit ADC, a 16 MHz clock and 4 UARTs (hardware serial ports). The Arduino Mega 2560 contains 256 kB of Flash Memory, 8 kB of SRAM and 4 kB of EEPROM. The Arduino family of microcontrollers comes with its own development environment and is also preloaded with a bootloader so no external hardware other than a USB cable is necessary to program the microcontroller.

When power is applied to the EET, the microcontroller will issue an initialization sequence. This includes serial ports for data transmission to the personal computer and the digital motor controllers being opened and respective baud rates being set. The baud rate for all serial data transmission is 115200 bps. All motors are then enabled and moved to a predefined zero position. This is so the actuators will start at the same position each time a test is run. Now, the EET is initialized and the reproduction of waveforms can begin. When the serial connection is established with the front end, an interrupt service routine is executed and the firmware begins playback.

The microcontroller firmware performs several important tasks. First, the microcontroller handles all timing peripherals for the simulator. A 16-bit periodic timer interrupt service routine is implemented to give precise timing parameters to the simulator. This controls the rate at which all actuation is updated. In this manner, all timing issues (such as jitter) that may arise by using a non-real-time OS (such as Microsoft Windows) are resolved, as exact timing is maintained using hardware timers on the microcontroller.

The microcontroller firmware buffers the short recordings of data that it requests from the PC on internal memory. When a new data burst is received, each sample is read and stored in a buffer consisting of four states. A ring buffer is implemented to buffer the data stream with a static data size of 120 samples. This buffer has first-in first-out (FIFO) characteristics so that the values inside the buffer are released in chronological order. Relative read and write indices are implemented. This is so elements in the array will not get overwritten and the read and write indices will never point to the same element. This provides a robust way of buffering the data stream. When an actuation update command is issued to the motor controllers and GSR simulator, the number of items queued in the buffer is checked. If the number of items queued in the buffer is below a threshold, then the microcontroller will write a status flag to the serial port to request more data from the personal computer. Figure 3 gives a high level abstraction of the microcontroller firmware.

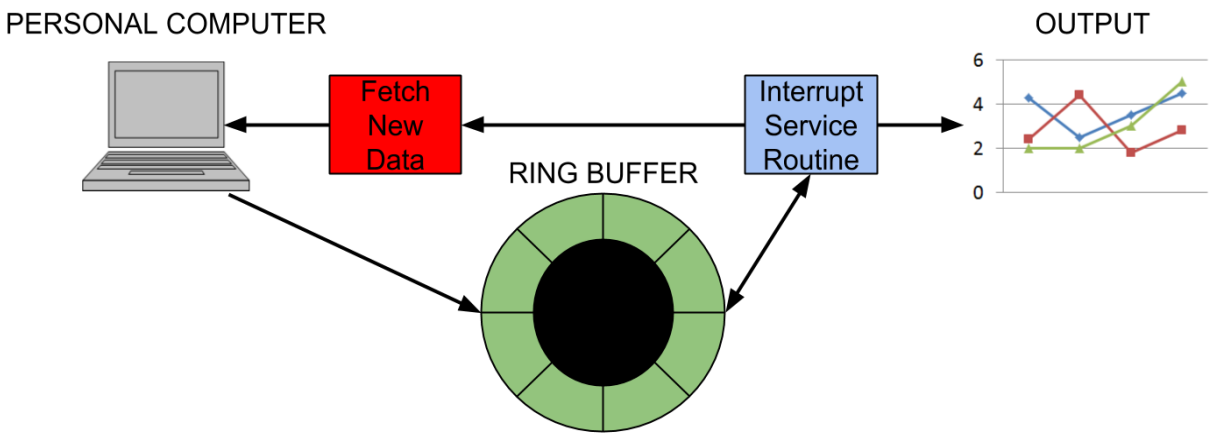

Figure 3. Abstraction of Microcontroller Firmware

To issue position control commands to the motor controllers, a low level programming protocol is used in which serial communication packets are issued over a RS232/RS485

communication network. A MAX485 chip [11] is used to convert serial communication data from RS232 protocol to RS485 protocol. The structure of the serial communication data packets includes header bytes, data bytes and tail bytes. Two error checking methods that are in place include two cyclic redundancy check (CRC) bytes and byte stuffing. A detailed look at the structure of the data packets are depicted in Table 2. A simple function within the microcontroller firmware is used to take a data point on the waveform and construct the serial communication packets necessary to control the actuators reproducing the waveform.

Table 2. Structure of Serial Communication Data Packet for Motor Controllers

Header	**Slave ID**	**Frame Type**	**Data**	**CRC**		**Tail**
0xAA 0xCC	1 byte	1 byte	0~248 bytes	2 bytes		0xAA 0xEE
				Low byte	High byte	

The microcontroller also directly controls the binary switch-based circuit used for the GSR channel. This channel is controlled using two digital ports (16 digital I/O pins) from the microcontroller configured as digital outputs. The microcontroller receives a resistance value and converts this into a 16-bit binary value implemented across two digital ports. In turn, digital signals from the microcontroller enable and disable switches in parallel with various resistance values to change the overall resistance of the circuit. More details of the GSR channel can be found in Section 3.2.

CHAPTER 3

HARDWARE SPECIFICATIONS AND IMPLEMENTATION

The EET features four physiological channels: one electrical circuit channel controlling the actuation of the electrodermal simulator and three electromechanical channels controlling the actuation of the respiratory and cardiovascular channels. Implementation details of each subsystem will be discussed.

3.1 Controller Board

The controller board houses several components crucial to the operation of the EET. The controller board contains the microcontroller, the electrodermal simulator circuit, power regulation circuit and interfaces to the personal computer and the digital motor controllers. As previously mentioned, the interface to the personal computer is configured through the USB port on the Arduino Mega2560. The interface to the digital motor controllers is an RJ-45 jack embedded onto the controller board. The MAX485 converter chip is housed here as well. Each digital motor controller is daisy-chained in an RS-485 network. Therefore, only one RJ-45 jack is needed to interface with the electromechanical subsystems. A picture of the controller board is depicted in Figure 4.

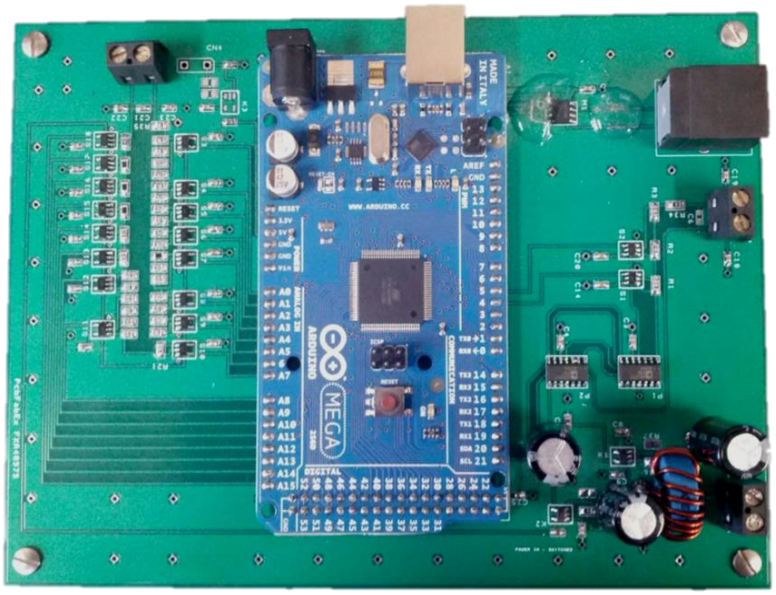

Figure 4. EET Controller Board

3.2 Electrodermal Simulator

The electrodermal simulator subsystem reproduced GSR signals originating from the conductivity of the skin. It was implemented using a binary switch-based resistive circuit. Digital ports F and K (corresponding to pins A0 – A15) configured as digital outputs on the ATmega2560 microcontroller were used to control the 16-bit binary resistive circuit. The entire resistive range, up to 4.096 MOhm, was implemented using a series of resistors enabled by 74V1G66STR digital switches [12]. The microcontroller converts the raw resistance value into a 16-bit binary value implemented across the two digital ports. In turn, digital signals from the microcontroller enable and disable switches in parallel with various resistance values to change the overall output resistance of the circuit.

A switch-based resistive circuit proved to create lower transient noise during resistance transitions than commercially available digital potentiometers. This was proven during the design and testing phase and verified via oscilloscope. The 16-bit digitization of the simulated

skin resistance allows for 64 Ohm resolution, which is negligible compared to the typical values (KOhms or more) of skin resistance [13]. The output leads of the electrodermal simulator are connected to two BNC connectors. On the end of the BNC connectors are snap buttons, to which the finger clips of the polygraph instrument attach. Due to the high impedance of the GSR channel, it is particularly sensitive to switching noise that may leak from the power supply or digital communication lines during switching transitions. To reduce transient and switching noise, an LC circuit was used to reduce noise from the power supply and a TI TPS79147 low-dropout regulator [14] with power supply rejection ratio of 70 dB at 10 kHz was used to provide regulated power to the V_{CC} pin of the switches. Digital noise from USB communications was reduced by using an Acromag USB isolator [15].

3.3 Respiratory Simulator

The respiratory subsystem reproduced respiratory signals induced by the expansion and contraction of the pneumatic respiratory sensors as the test subject inhales and exhales. This subsystem contained two identical channels providing mechanical excitation to the abdominal and thoracic pneumatic respiratory sensors. Each channel was identically implemented as a digitally controlled linear actuator driven by an Ezi-Servo EzM-42-XL-A stepper motor [16]. This is a high-precision and high-speed stepper motor providing 10,000 pulses per revolution of angular position feedback. The digital motor controller was a FASTECH Ezi-Servo Plus-R motor drive [16] that accepted commands via an RS485 interface from the microcontroller. The angular position commands were issued to the closed-loop position controller for the motor, which drove a lead screw linear actuator with a 10.16 mm screw lead and an available 121 mm stroke length [17]. One end of the pneumatic pressure sensor was attached to the carriage on the actuator while the other end of the pneumatic pressure sensor was attached to a stationary

support. A sizing chain that is found on the majority of pneumatic pressure sensors attaches to the stationary support to accommodate for various sizes of pressure sensors. The respiratory subsystem implementation is shown in Figure 5 below.

Figure 5. Respiratory Channels with Pneumatic Pressure Sensors Attached

Each position command issued to the motor controller caused the pneumatic pressure sensor to expand and contract to simulate respiratory movement. Note that while the angular motor position was controlled in a closed-loop manner by the motor controller, the position feedback loop was not closed on the linear displacement of the actuator carriage. In a reasonable assumption, all mechanical dynamics from the motor shaft to the air pressure transducer on the polygraph instrument were neglected.

For the purposes of sizing the motor and determining the screw lead during the design process, a sinusoidal desired position was assumed with the maximum peak-to-peak displacement of 5 cm and a frequency, f_r, of 0.5 Hz. In this case, the frequency of the sinusoidal desired position is denoted as:

$$\boldsymbol{\omega_r = 2\pi * f_r = 2\pi * 0.5 = \pi\, rad/s} \quad (1)$$

The upper limit required from the system requirements must be met by the motor and linear actuator. With this extreme case in mind, the position, velocity and acceleration profiles were created.

$$x_r = 5\sin(\omega_r t) = 5\sin(\pi t)\ cm \tag{2}$$

$$v_r = \frac{dx_r}{dt} = 5\pi\cos(\pi t)\ \ cm/s \tag{3}$$

$$a_r = \frac{d^2x_r}{dt^2} = \frac{dv_r}{dt} = -5\pi^2\sin(\pi t)\ \ cm/s^2 \tag{4}$$

Based on these profiles, $v_{r,max}$= 0.016 m/s and $a_{r,max}$= 0.494 m/s^2. The acceleration profile, along with actuator friction and carriage mass, m_c, dictated the maximum required linear force.

$$F = m_c a_r = (0.06)(0.494) = 0.03\ N \tag{5}$$

The load acquired from the pneumatic pressure sensors was negligible. This force and velocity data was sufficient to find a screw lead and motor such that the requirements were within the torque speed curve of the motor. Of the screw leads available, a 10.16 mm screw lead was chosen.

$$Fv_r = T\omega_r \tag{6}$$

$$T = F\frac{v_r}{\omega_r} = F\frac{l}{2\pi} = \frac{(0.03)(0.0106)}{2\pi} = 3.2 * 10^{-4}\ N - m = 0.32\ mN - m \tag{7}$$

The selected motor provides a maximum torque of 650 mN-m and is capable of delivering 20 mN-m of torque at a speed of 3,000 rpm, which corresponds to a linear velocity of 50 cm/s.

3.4 Cardiovascular Simulator

The cardiovascular subsystem reproduced cardiovascular signals induced by pulses from the brachial artery against the cuff of the sphygmomanometer. The cardiovascular simulator consisted of a single channel providing mechanical excitation to the cuff of the sphygmomanometer. It was implemented as a digitally controlled linear actuator similar but not identical to that of the respiratory channels. The controller accepted angular position commands, which drove a lead screw linear actuator with a 5mm screw lead and an available 71 mm stroke length. Typical cardiovascular waveforms required short linear displacements at a relatively high frequency. As with the respiratory channels, the angular position of the motor was controlled in a closed-loop manner by the motor controller, but there was no active position feedback of the linear displacement of the actuator carriage.

A custom sphygmomanometer cuff support was used to simulate cardiovascular activity in the brachial artery (Figures 6 and 7). A stationary support (Figure 6, left) contains a half-cylinder made of PVC plastic that is attached across two beams. The mobile support (Figure 6, right) consists of a horizontal half-cylinder mounted to the carriage of the linear actuator. Linear displacement of the mobile support creates a proportional change in the cuff's air pressure.

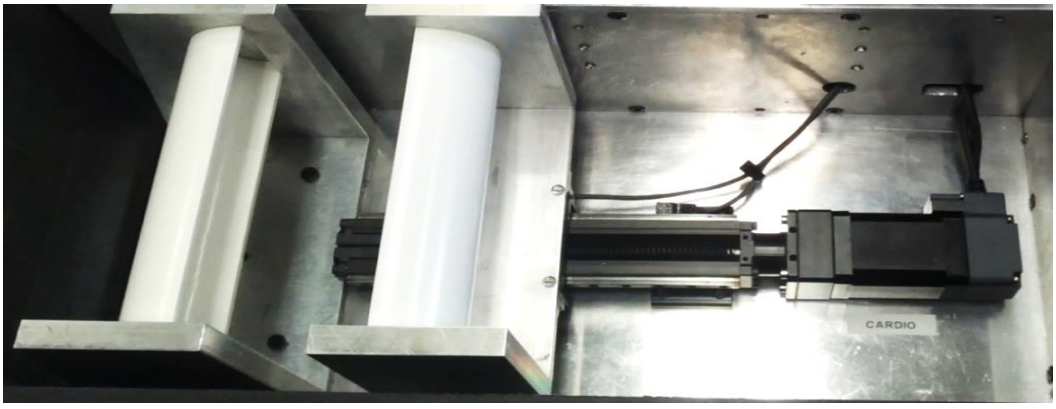

Figure 6. Cardiovascular Channel Implementation

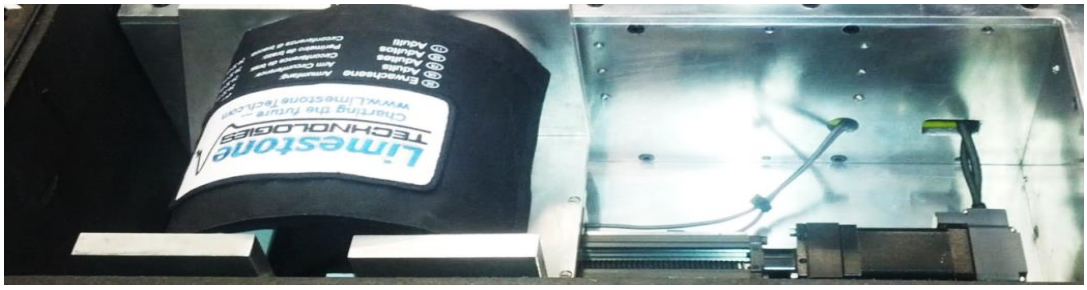

Figure 7. Cardiovascular Subsystem with Sphygmomanometer Cuff Attached

Each position command issued to the motor controller caused the cuff to expand and contract to simulate cardiovascular activity. The implemented configuration of the cardiovascular channel supports ensures that an evenly distributed force is applied to the cuff, minimizing bend and flex within the supports. The large carriage mount and side rails aide in reducing bend and flex within the supports while running the simulator at high frequencies and amplitudes.

To determine the size of the motor and screw lead for the cardiovascular channel, a sinusoidal desired position was assumed with the maximum peak-to-peak displacement of 5 mm and a frequency, f_c, of 3.33 Hz.

$$\omega_c = 2\pi * f_c = 2\pi * 3.33 = \frac{20\pi}{3}\ rad/s \tag{8}$$

From this information, position, velocity and acceleration profiles were created for the cardiovascular channel.

$$x_c = 5\sin(\omega_c t) = 5\sin(\frac{20\pi}{3}t)\ mm \tag{9}$$

$$v_c = \frac{dx_c}{dt} = \frac{100\pi}{3}\cos\left(\frac{20\pi}{3}t\right)\ mm/s \tag{10}$$

$$a_c = \frac{d^2x_c}{dt^2} = \frac{dv_c}{dt} = -\frac{2000\pi^2}{9}\sin\left(\frac{20\pi}{3}t\right)\ mm/s^2 \tag{11}$$

Based on these profiles, $v_{c,max}$= 0.105 m/s and $a_{c,max}$= 2.19 m/s^2. Because the EET must be able to accommodate pressures up to 200 mmHg, the load acquired from the pressure cuff on the cardiovascular channel cannot be neglected. It was experimentally determined that the maximum required linear force for the cardiovascular channel would be 275.8 N. This force and velocity data was sufficient to find a screw lead and motor such that the requirements were within the torque speed curve of the motor. A 5 mm screw lead was chosen for the cardiovascular channel.

$$Fv_c = T\omega_c \tag{12}$$

$$T = F\frac{v_c}{\omega_c} = F\frac{l}{2\pi} = \frac{(275.8)(0.005)}{2\pi} = 0.219\ N-m = 219\ mN-m \tag{13}$$

As previously mentioned the selected motor for the respiratory channels provided a maximum torque of 650 mN-m and is capable of delivering 20 mN-m of torque at a speed of 3,000 rpm, which corresponds to a linear velocity of 50 cm/s. This motor was also selected for the cardiovascular channel. Based on the screw lead, torque, velocity and acceleration requirements, it is satisfactory to use the same motor and motor controller in all electromechanical channels. Using the same motor is preferable for consistency throughout the system.

3.5 Full System Integration

Figure 8 shows the assembled prototype of the EET. The actuator and supports labeled (a) belong to the thoracic respiratory channel. The actuator and supports labeled (b) belong to the abdominal respiratory channel. The cardiovascular channel is labeled (c) and the GSR

channel is labeled (d). Each electromechanical channel actuator is mounted directly to a custom base frame which fits inside the Pelican 1610 case [18] shown in Figure 8. All other components of the EET including the controller board, power supplies and motor controllers are mounted to the underside of the base frame. This design allows for safe and efficient transportation of the EET.

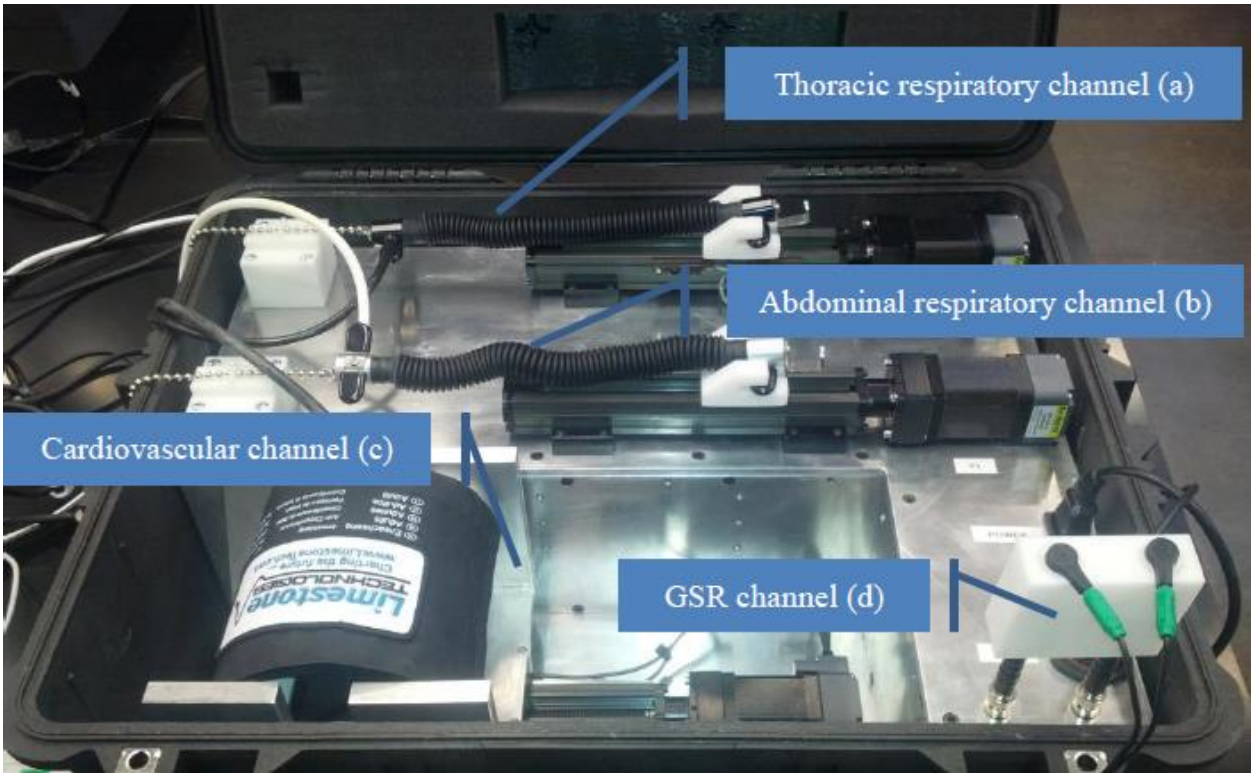

Figure 8. Fully Assembled EET

3.5.1. System Power

Three separate AC-DC rectifier power supplies were used to power the EET. A 24V, 240W AC-DC power supply was used to power the digital motor controllers and DC motors used in the electromechanical channels. The maximum current consumption for the motor drive is 500mA per drive. The current consumption for the motor is 1.2A per phase (bi-polar). This

would bring the total maximum current consumption for the three electromechanical channels to 5.1A. A 12V, 10W AC-DC power supply was used to power the Arduino Mega2560. The Arduino Mega2560 board can operate on an external power supply of 6-20V with the recommended range being 7 to 12 volts. A voltage regulator on the Arduno Mega2560 regulates the operating voltage of the microcontroller to 5V. A 5V, 7.5W AC-DC power supply was used to generate the supply voltage used by the digital switches in the electrodermal simulator.

CHAPTER 4

VALIDATION TESTS AND RESULTS

The EET was validated in a series of tests evaluating accuracy and repeatability of the reproduction of varying input signals. Reference computer-generated signals and human recordings obtained on a polygraph were played back on the EET. The signals reproduced by the EET were recorded using an LX4000 Computerized Polygraph [19] made by Lafayette Instruments using Lafayette Polygraph System LX software version 11.1.4 and formatted to proprietary DACA file format using pREFORMAT Software Version 1.02. This particular polygraph instrument has a sample rate of 30 samples per second for each sensor.

When each vendor polygraph file is reformatted to the DACA file format, each file is converted to a relative scale ranging from 0 – 10,000 DACA units. Because these values are dimensionless, there is no universal conversion from DACA formatting to physical values. Rather, an individual linear transformation must be computed for each file. Default scaling for the playback of human recordings is set to each DACA unit corresponded to approximately 5 pulses of the stepper motor for the respiratory channels, 1 pulse of the stepper motor for the cardiovascular channel and approximately 410Ω for the GSR channel. Thus, the peak-to-peak amplitude of 10,000 DACA units translates to 50.8mm physical displacement of the carriage on the linear actuator for the respiratory channel, 5mm physical displacement of the carriage on the linear actuator for the cardiovascular channel and range of 4.1M Ω for the GSR channel.

4.1 Validation Test Suite Format

The test suite used to validate the EET consisted of 9 computer generated signals and 1 human recording. Each of the 9 computer generated signals and the human recording were run 10 times each. The set of computer generated signals consisted of sinusoids with varying peak-to-peak amplitudes and frequencies for each channel. For all amplitudes, each separate channel was run at 3 varying frequencies. The amplitudes of the sinusoids covered 80, 40 and 20 percent of the full dynamic range for each channel. Table 3 shows the peak-to-peak amplitude and frequency range for each channel.

Table 3. Amplitude and Frequency Range for Computer-Generated Signals

Simulator channel	**Amplitude**	**Frequency**
Galvanic skin response	840kΩ	0.25 Hz
	1.68MΩ	0.5 Hz
	3.36MΩ	1 Hz
Respiratory	10mm	0.1 Hz
	20mm	0.3 Hz
	40mm	0.5 Hz
Cardiovascular	1.25mm	0.667 Hz
	2.5mm	2 Hz
	5mm	3.333 Hz

The amplitudes and frequency ranges were carefully chosen to demonstrate the lower and upper limits of the simulator based on the system requirements. These frequencies are typical lower and upper limits of human capabilities. For the GSR channel, the response is usually a long lasting waveform of a simple shape [20] with small variations in resistance compared to the entire resistive range [6]. These smaller variations in resistance usually occur at a higher frequency than a variation that will cover a large resistive range. The set of test signals includes large variations in resistance; therefore, it is sufficient to test the EDA channel at lower

frequencies. The normal breathing rate for an adult is approximately 14 breaths per minute, or 0.233 Hz [21]. The frequencies chosen for the respiratory channel is representative of the typical breathing rate for an adult. A maximum displacement of 40mm is adequate for the displacement seen by an adult wearing a pneumatic breathing sensor. The frequency range tested on the cardiovascular channel is also representative of typical physiological processes of an adult. As proven with demonstrations and testing, a maximum linear displacement of 5mm for the cardiovascular channel is satisfactory to accurately reproduce waveforms being played on the EET. Initially, the cuff is inflated to a pressure of 60mmHg. With this initial pressure, a linear displacement of 5mm produces an output of approximately 120mmHg. Obviously, different initial pressures will cause different pressure outputs.

The human recording consisted of different waveforms in all channels of the recording. The human recording was obtained from a sample recording provided with the polygraph used in the experiments. Each physiological signal in the human recording falls within a typical range for amplitude as well as frequency for each respective channel.

4.2 Test Evaluation Statistics

The purpose of the validation test suite was to test the accuracy and repeatability of the EET. This also provides validation for the EET that it is capable of reproducing physiological signals with high precision and accuracy. As a method to do this, several statistics evaluating accuracy and repeatability were obtained from the data.

4.2.1 Accuracy Evaluation

Accuracy of the reproduction was evaluated as absolute average error E_{REF}. The reference signals (DACA files played on the EET) were aligned in time with the recordings captured on the polygraph (further referred as test signals) and trimmed to identical length (160 seconds for computer-generated test signal recordings, and 275 seconds for the human recording). The E_{REF} was computed as an average of the absolute difference between the reference and test signals averaged over 10 experiments:

$$E_{REF} = \frac{1}{N}\sum_{N}\left(\frac{\sum_{1}^{M}|x(t)-r(t)|}{M}\right), \quad (14)$$

where N=10 the is number of experiments, M is the length of a recording, x(t) is the test signal and r(x) is the reference signal.

4.2.2 Repeatability Evaluation

Repeatability of the reproduction was evaluated in several ways. First, to disregard any differences between the reference and test signals caused by the transfer characteristics of the polygraph, absolute average error E_{MEAN} was computed as:

$$E_{MEAN} = \frac{1}{N}\sum_{N}\left(\frac{\sum_{1}^{M}|x(t)-m(t)|}{M}\right), \quad (15)$$

where m(t) is the mean signal obtained by point-to-point averaging of the test signals aligned in time,

$$m(t) = \frac{1}{N}\sum_{N} x(t). \quad (16)$$

The absolute average error evaluates the average point-to-point error between each test signal and the mean signal obtained by point-to-point averaging of the test signals aligned in time. Second, average standard deviation of the test signals relative to their mean was computed as

$$STD_{MEAN} = \frac{1}{N}\sum_{N} std(|x(t) - m(t)|) \quad (17)$$

to quantify how much dispersion from the average test signal exists.

4.3 Results from the Validation Test Suite

Figures 9 – 15 demonstrate the comparison of recorded signals being played back on EET (original signals) vs. signals captured from the EET by the polygraph (reproduced signals). A few charts from each channel were chosen to visually show a subset of the reproduction of signals on the EET. By visual comparison, it is clear that the difference between the original and the reproduced signals is minimal.

4.3.1 Electrodermal Simulator Results Summary and Discussion

The summary of errors representing accuracy and repeatability of reproduction for computer-generated signals is shown in Table 4 for the galvanic skin response channel. A partial recording of a test series for the galvanic skin response channel is shown in Figure 9.

Table 4. Results for Computer-Generated Simulation of Galvanic Skin Response

Actuation range		**Frequency**		
		0.1 Hz	0.5 Hz	1 Hz
840 kOhm	E_{REF}	116.4 (1.16 %)	175.3 (1.75 %)	194.8 (1.95 %)
	E_{MEAN}	61.8 (0.62 %)	83.9 (0.84 %)	94.5 (0.95 %)
	STD_{MEAN}	48.7 (0.49 %)	69.1 (0.70 %)	79.6 (0.80 %)
1.68 MOhm	E_{REF}	236.2 (2.36 %)	286.6 (2.87 %)	288.2 (2.88 %)
	E_{MEAN}	97.1 (0.97 %)	169.3 (1.69 %)	154.3 (1.54 %)
	STD_{MEAN}	85.3 (0.85 %)	142.0 (1.42 %)	173.4 (1.73 %)
3.36 MOhm	E_{REF}	346.6 (3.47 %)	321.8 (3.22 %)	398.4 (3.98 %)
	E_{MEAN}	137.9 (1.38 %)	150.9 (1.51 %)	290.5 (2.90 %)
	STD_{MEAN}	133.4 (1.33 %)	117.5 (1.18 %)	231.1 (2.31 %)

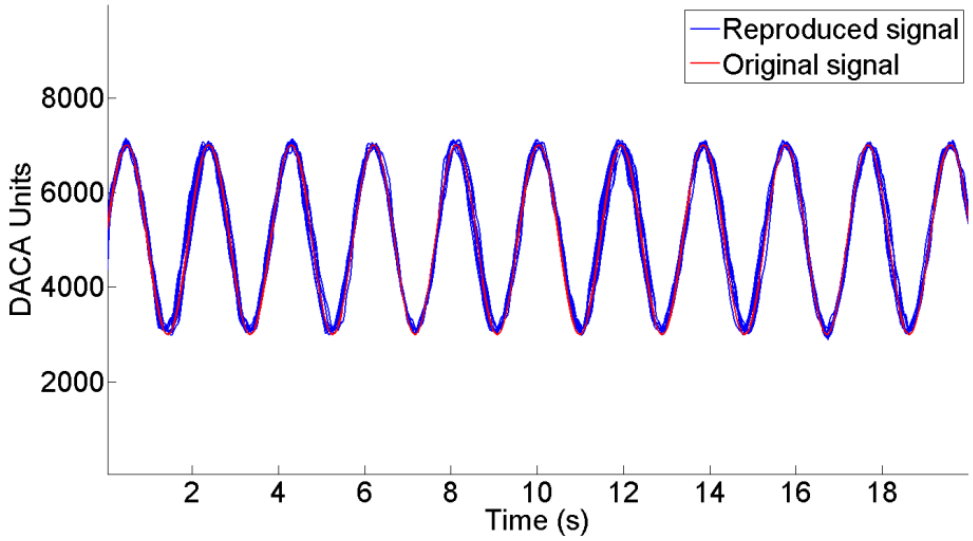

Figure 9. Partial Recording of Sinusoid of 1.68MOhm Actuation Range at 0.5 Hz for GSR Channel

The average absolute error between each test signal and the reference signal for the GSR simulator was 1.16% for the signal with the lowest amplitude and frequency and 3.98% for the signal with the largest amplitude and highest frequency. The GSR simulator proved to be highly repeatable with the largest amplitude and highest frequency signal producing an average absolute error between each test signal and the mean test signal of 2.90%.

4.3.2 Respiratory Simulator Results Summary and Discussion

The summary of errors representing accuracy and repeatability of reproduction for computer-generated signals is shown in Table 5 for the respiratory channel. A partial recording of a test series for the respiratory channel is shown in Figure 10.

Table 5. Results for Computer-Generated Simulation of Respiratory Activity

Actuation range		**Frequency**		
		0.1 Hz	0.3 Hz	0.5 Hz
10 mm	E_{REF}	71.4 (0.71 %)	92.3 (0.92 %)	112.9 (1.13 %)
	E_{MEAN}	61.4 (0.61 %)	84.5 (0.85 %)	92.3 (0.92 %)
	STD_{MEAN}	43.6 (0.43 %)	59.6 (0.60 %)	64.8 (0.65 %)
20 mm	E_{REF}	85.4 (0.85 %)	188.0 (1.88 %)	212.8 (2.13 %)
	E_{MEAN}	47.6 (0.48 %)	131.1 (1.31 %)	210.4 (2.10 %)
	STD_{MEAN}	49.2 (0.49 %)	100.7 (1.01 %)	166.1 (1.66 %)
40 mm	E_{REF}	195.2 (1.95 %)	217.6 (2.18 %)	374.1 (3.74 %)
	E_{MEAN}	94.1 (0.94 %)	131.3 (1.31 %)	367.9 (3.68 %)
	STD_{MEAN}	75.1 (0.75 %)	112.6 (1.13 %)	290.9 (2.91 %)

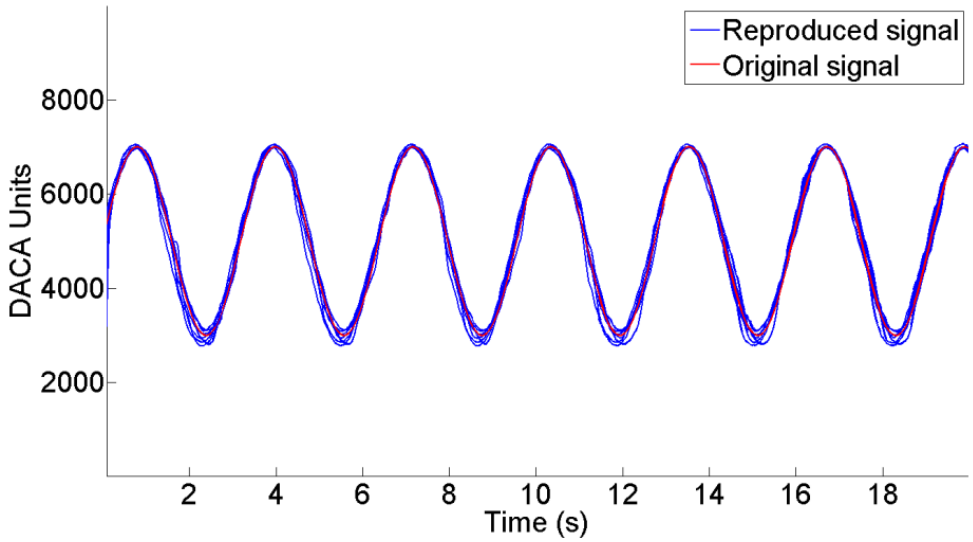

Figure 10. Partial Recording of Sinusoid of 20mm Actuation Range at 0.3 Hz for Respiratory Channel

The respiratory channel proved to be the most accurate subsystem on the EET. The average absolute error between each test signal and the reference signal for the respiratory subsystem was 0.71% for the signal with the lowest amplitude and frequency and 3.74% for the signal with the largest amplitude and highest frequency. The respiratory channel also proved to

be very repeatable with the largest value for E_{MEAN} being 3.68% and the largest value for STD_{MEAN} being 2.91%.

4.3.3 Cardiovascular Simulator Results Summary and Discussion

The summary of errors representing accuracy and repeatability of reproduction for computer-generated signals is shown in Table 6 for the cardiovascular channel. A partial recording of a test series for the cardiovascular channel is shown in Figure 11.

Table 6. Results for Computer-Generated Simulation of Cardiovascular Activity

Actuation range		**Frequency**		
		0.667 Hz	2 Hz	3.333 Hz
1.25 mm	E_{REF}	109.7 (1.10 %)	187.6 (1.88 %)	504.3 (5.04 %)
	E_{MEAN}	62.3 (0.62 %)	93.6 (0.94 %)	317.4 (3.17 %)
	STD_{MEAN}	43.9 (0.43 %)	79.3 (0.79 %)	295.7 (2.96 %)
2.5 mm	E_{REF}	212.5 (2.12 %)	301.7 (3.02 %)	694.9 (6.95 %)
	E_{MEAN}	175.8 (1.76 %)	189.6 (1.90 %)	382.5 (3.83 %)
	STD_{MEAN}	112.6 (1.13 %)	162.2 (1.62 %)	312.2 (3.12 %)
5 mm	E_{REF}	258.9 (2.59 %)	341.8 (3.42 %)	1217.5 (12.18 %)
	E_{MEAN}	145.3 (1.45 %)	170.9 (1.71 %)	487.0 (4.87 %)
	STD_{MEAN}	116.6 (1.17 %)	143.5 (1.44 %)	392.1 (3.92 %)

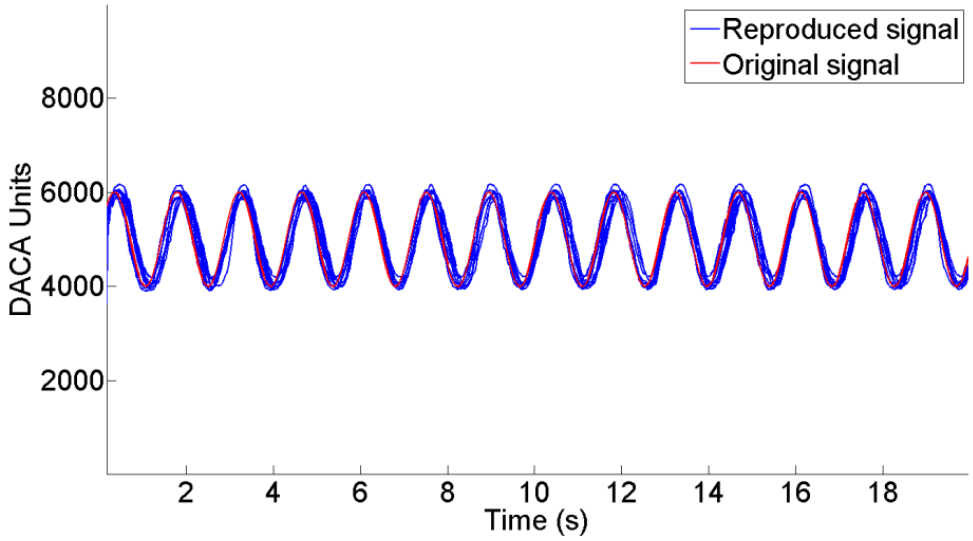

Figure 11. Partial Recording of Sinusoid of 1.25mm Actuation Range at 0.667 Hz for Cardiovascular Channel

The cardiovascular channel proved to be the least accurate and repeatable. This is partly due to the fact that the actuation rate is much higher for the cardiovascular channel than the respiratory and GSR channels. For the test signal with the largest amplitude and highest frequency, E_{REF} was 12.18% while E_{MEAN} and STD_{MEAN} were 4.87% and 3.92%, respectively. Another reason for the high error and standard deviation percentages is the relatively low sample rate of the polygraph (30 Hz). This may not be sufficient for accurate representation of high-frequency inputs. Figure 12 illustrates the under-sampling by the polygraph by demonstrating the signal captured on the cardiovascular channel with the maximum amplitude (5mm) and frequency of 3.333 Hz. The original signal being played can be seen in Figure 13. Although the physical linear displacement did not vary per sinusoidal cycle, it appears to vary on the graph.

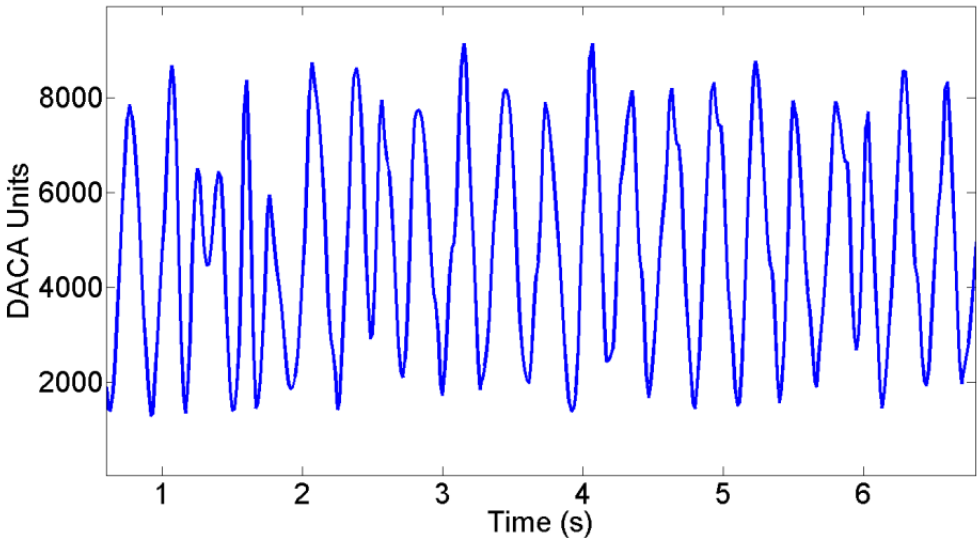

Figure 12. Partial Recording of Sinusoid of 5mm Actuation Range at 3.333 Hz for Cardiovascular Channel

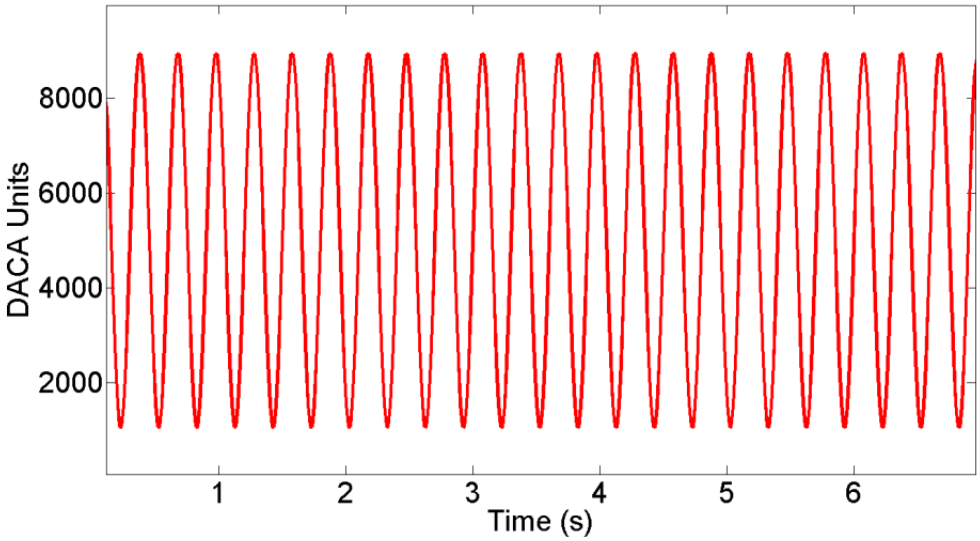

Figure 13. Partial Reference Signal of Sinusoid of 5mm Actuation Range at 3.333 Hz for Cardiovascular Channel

4.3.4 Physiological Recording Results and Discussion

Figures 14-16 demonstrate the comparison of recorded signals being played back on EET (original signals) vs. signals captured from the EET by the polygraph (reproduced signals) for the human recording. Table 7 provides a summary of error representing accuracy and repeatability of reproduction for human recorded signals for all EET channels.

Table 7. Error Results for Previously Recorded Physiological Signals on All EET Channels

Channel		**Error Measure**
GSR channel	E_{REF}	101.7 (1.02 %)
	E_{MEAN}	59.6 (0.60 %)
	STD_{MEAN}	27.8 (0.28 %)
Respiratory Channel	E_{REF}	157.9 (1.58 %)
	E_{MEAN}	26.4 (0.26 %)
	STD_{MEAN}	159.7 (1.60 %)
Cardiovascular Channel	E_{REF}	209.2 (2.09 %)
	E_{MEAN}	91.8 (0.92 %)
	STD_{MEAN}	180.1 (1.80 %)

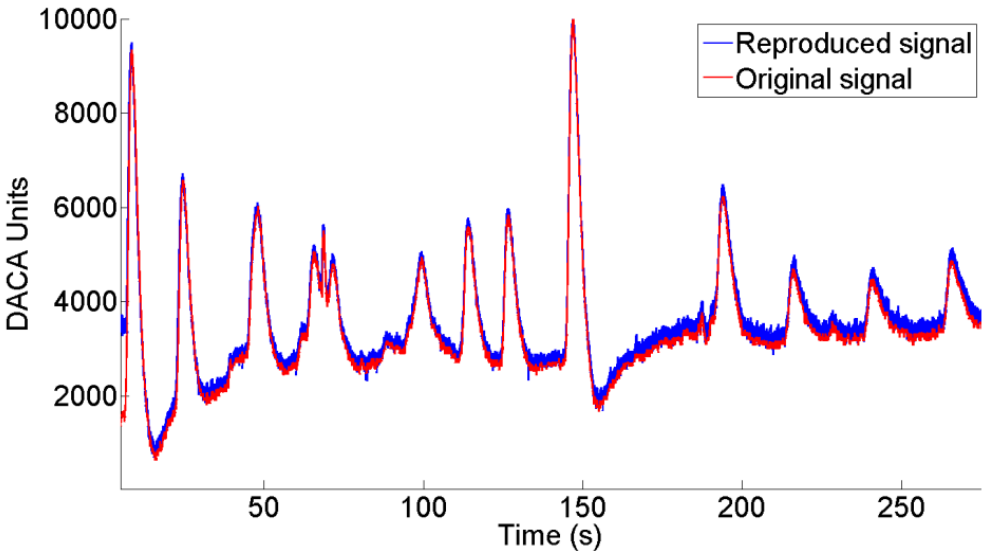

Figure 14. Full-Length Human recording of the GSR channel

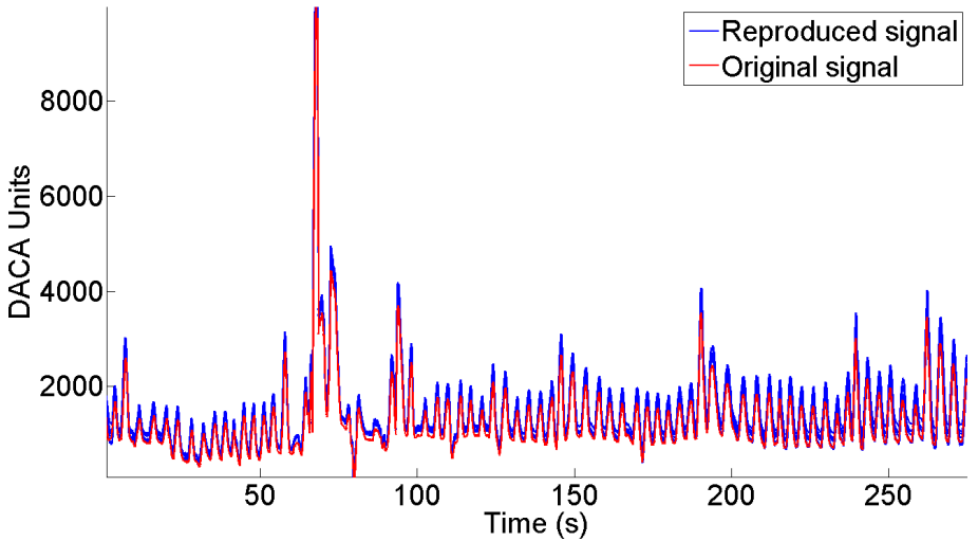

Figure 15. Full-Length Human Recording of Respiratory Channel

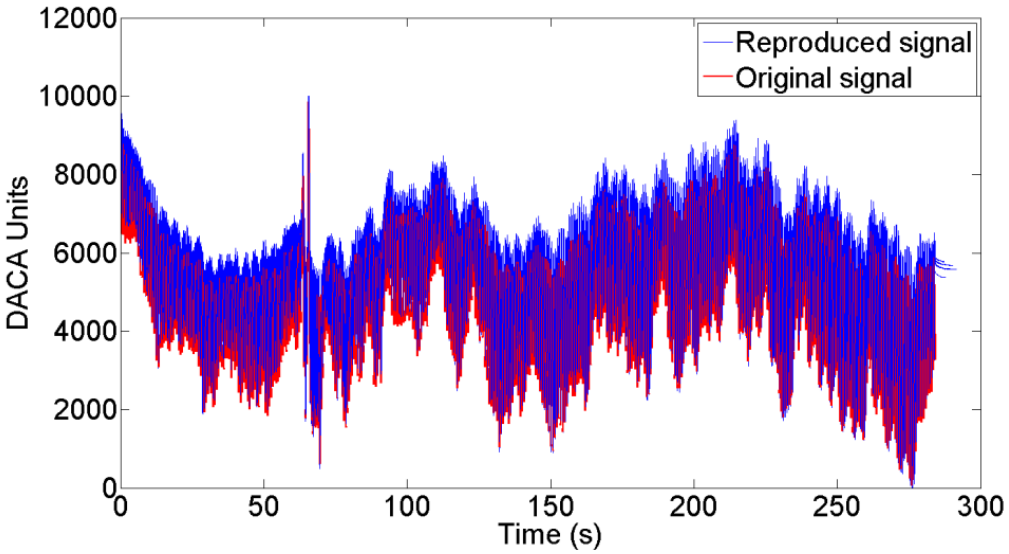

Figure 16. Full-Length Human Recording of the Cardiovascular Channel

The accuracy and repeatability of the EET for a previously recorded physiological signal input proved satisfactory for all channels. E_{REF} for the GSR channel was 1.02% while E_{REF} for

the cardiovascular channel was 2.09%. The respiratory channel proved more accurate than the cardiovascular channel with an E_{REF} of 1.58%. The respiratory channel provided the most repeatable signals with an E_{MEAN} of 0.26%. The validation tests proved the EET provides acceptable responses to a variety of inputs. The EET reproduces physiological signals with sufficient accuracy and repeatability.

CHAPTER 5

SYSTEM IDENTIFICATION AND COMPENSATOR DESIGN

Determined from the results and discussion presented in Chapter 4, the EET demonstrates its ability to reproduce both computer-generated signals and previously recorded physiological signals originating from the human body with sufficient accuracy and repeatability. At this point, the EET has shown an acceptable response to input signals to the system. However, there is a percent error distinguishing the input files played on the EET from the output charts captured by the polygraph when reproducing physiological signals. While it may not be plausible in a real world system to have an absolute zero percent error, the desirable system response is to have an error as close to zero as possible.

The most apparent way to improve the system response is to tune all pertinent system parameters. If performance requirements do not improve with the adjustment of system parameters, the system must be altered in some way to achieve the desired response. To achieve the desired system response for the electromechanical channels, it is necessary to introduce a compensator to the system [22]. The system identification methods, transfer function models and compensator designs presented in this chapter apply to the electromechanical respiratory and cardiovascular channels.

5.1 EET Electromechanical Subsystem Identification Models

From a transfer function model viewpoint, two system input/output relationships should be taken into consideration. The first is a relationship between the input to the EET and the linear displacement of the actuator carriage. The second is a relationship between the linear displacement of the actuator carriage and the output signal captured by the polygraph. These relationships apply directly to all electromechanical channels on the EET. This method of transfer function modeling approximates each single-input single-output subsystem as a linear time-invariant (LTI) system. Figure 17 provides a block diagram showing these relationships.

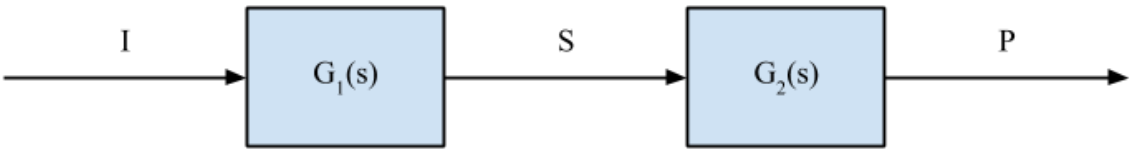

Figure 17. Block Diagram of Current System Model

The input signal to the system, I, provides position data to control the linear displacement of the actuator carriage, S. The actuator carriage's linear displacement position, S, provides direct physical excitation to the polygraph instrument, P. $G_1(s)$ is defined as the transfer function of the input signal and the linear displacement of the actuator carriage. $G_2(s)$ is defined as the transfer function of the linear displacement of the actuator and the output signal captured by the polygraph instrument. By representing $G_1(s)$ and $G_2(s)$ as cascading transfer functions, a full system transfer function $G(s)$ can be defined as follows:

$$G(s) = G_1(s) * G_2(s) = \frac{S}{I} * \frac{P}{S} = \frac{P}{I} \tag{18}$$

A compensator component, $G_C(s)$, can now be introduced to the input of the system model. Figure 18 presents a block diagram of the compensated system model. Before the compensator component $G_C(s)$ can be designed, transfer functions $G_1(s)$ and $G_2(s)$ need to be accurately defined.

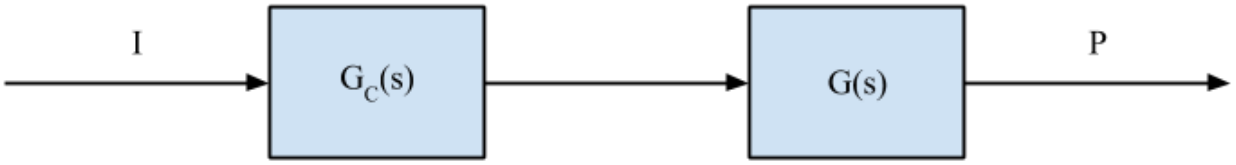

Figure 18. Compensated System Model

5.2 Determining the System Transfer Functions

To experimentally determine the frequency response of the system and gain further insight into the system transfer functions, the input signal to the EET, linear displacement of the actuator carriage and the output signal captured by the polygraph need to be synchronously recorded as a function of time. Though the linear position of the actuator carriage feedback loop was not closed, linear displacement was measured by a SoftPot linear potentiometer [23]. The potentiometer was strategically mounted so as to record the precise linear displacement of the actuator carriage as a function of time. The potentiometer was sampled at 120 Hz and digitized using a 10 bit ADC on an Arduino Mega2560 (separate from the Arduino Mega2560 handling the microcontroller firmware). Rather than read position data from the rotary encoder on the motor, a linear potentiometer was used because it can measure the exact displacement of the actuator carriage. Therefore, the dynamics from the motor shaft to the actuator carriage are not neglected in the system model. Thus, all input and output parameters in the system were able to be synchronously recorded to provide exact position data as a function of time.

Now that precise position data is available, the frequency response and transfer functions of the system can be determined. To accomplish this, input and output data was collected for input signals consisting of an impulse function, a step function, and a sinusoid of known frequency and amplitude. Though the amplitude of the input sinusoid did not vary, the frequency increased in steady increments from 0.1 Hz to 1 Hz for the both the respiratory channel and cardiovascular channel. This frequency range is included in the frequencies specified by the system requirements, but stays on the lower end of the spectrum for the cardiovascular channel. This is to keep the phase margin at a reasonable level for the sake of fitting a transfer function to the system. Due to the slow sample rate of the polygraph instrument, the system no longer remains linear with sinusoidal inputs of maximum magnitude and frequency. This was demonstrated by the validation tests in Chapter 4. The purpose of the transfer function being determined is to approximate a model of the system as accurately as possible at the frequencies covered by the EET. Any frequency outside of the system requirements that is modeled is extraneous.

By taking advantage of the various system identification and simulation tools in MATLAB [24], transfer functions were able to be determined using the input and output data captured during the experiments described above. The input and output signals were aligned in time (with a pulse at the start of the signal) before processing the data. MATLAB estimated transfer function coefficients based on a given time-domain data object created from corresponding input and output signals and a given relative order of the system. Figures 19 – 24 below demonstrate the time response for the respiratory and cardiovascular channels to the various inputs used to model the system.

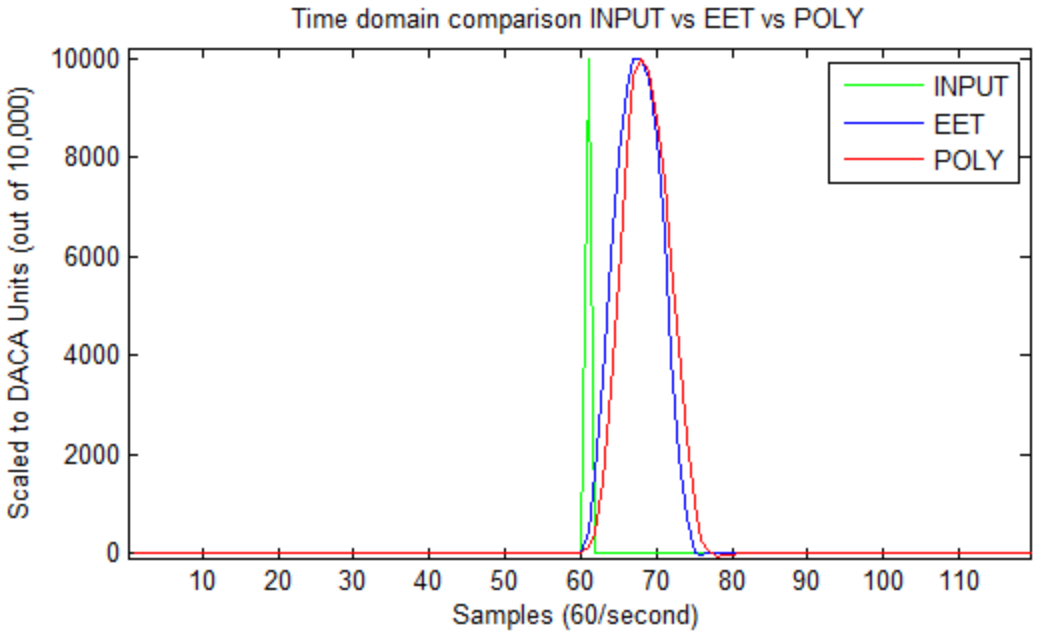

Figure 19. Time Domain Response for Input Signal, Linear Displacement of Actuator Carriage and Output Signal Captured by Polygraph to Impulse Input for Respiratory Channel

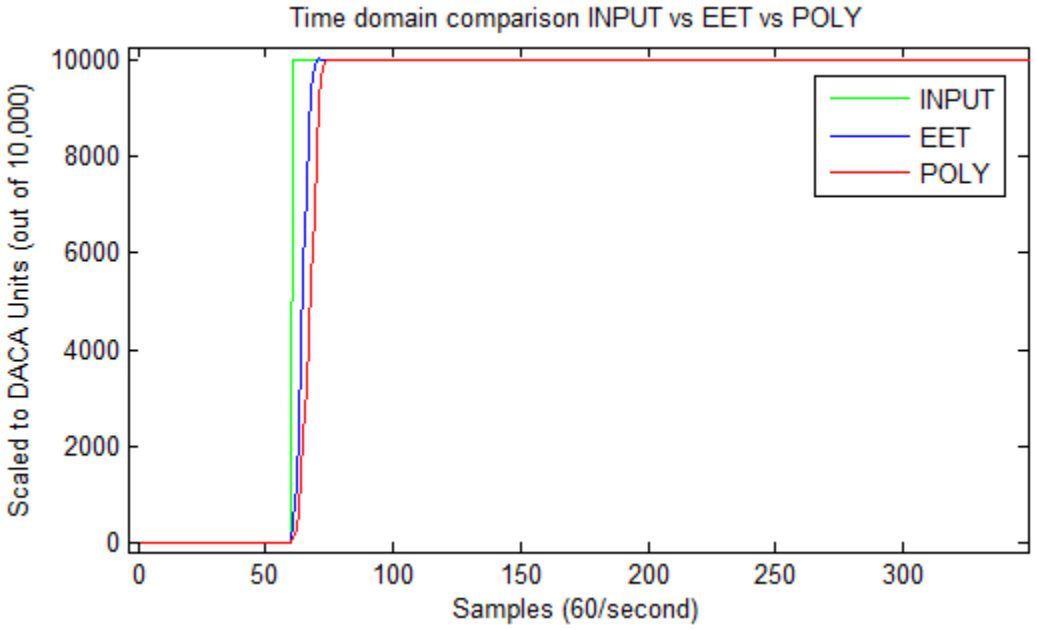

Figure 20. Time Domain for Input Signal, Linear Displacement of Actuator Carriage and Output Signal Captured by Polygraph Response to Step Input for Respiratory Channel

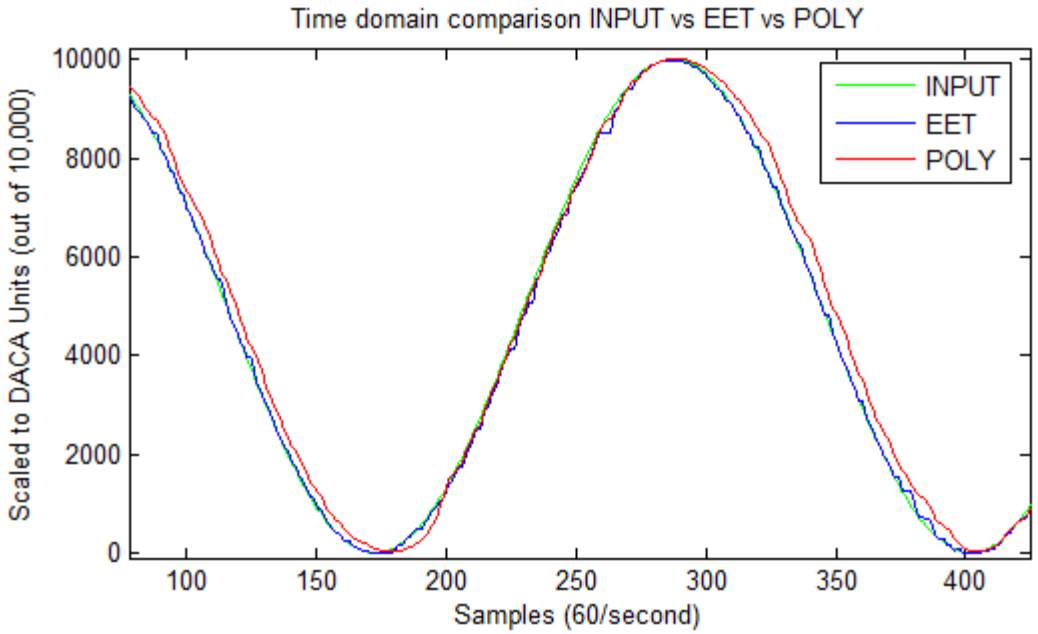

Figure 21. Scaled Time Domain Response for Input Signal, Linear Displacement of Actuator Carriage and Output Signal Captured by Polygraph to Sinusoid Input for Respiratory Channel

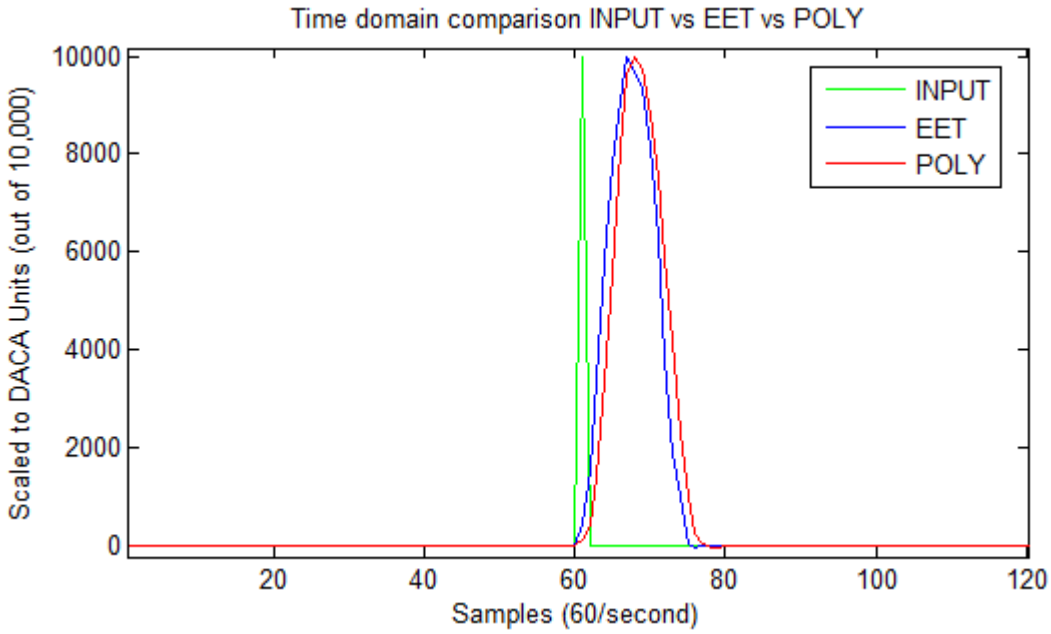

Figure 22. Time Domain Response for Input Signal, Linear Displacement of Actuator Carriage and Output Signal Captured by Polygraph to Impulse Input for Cardiovascular Channel

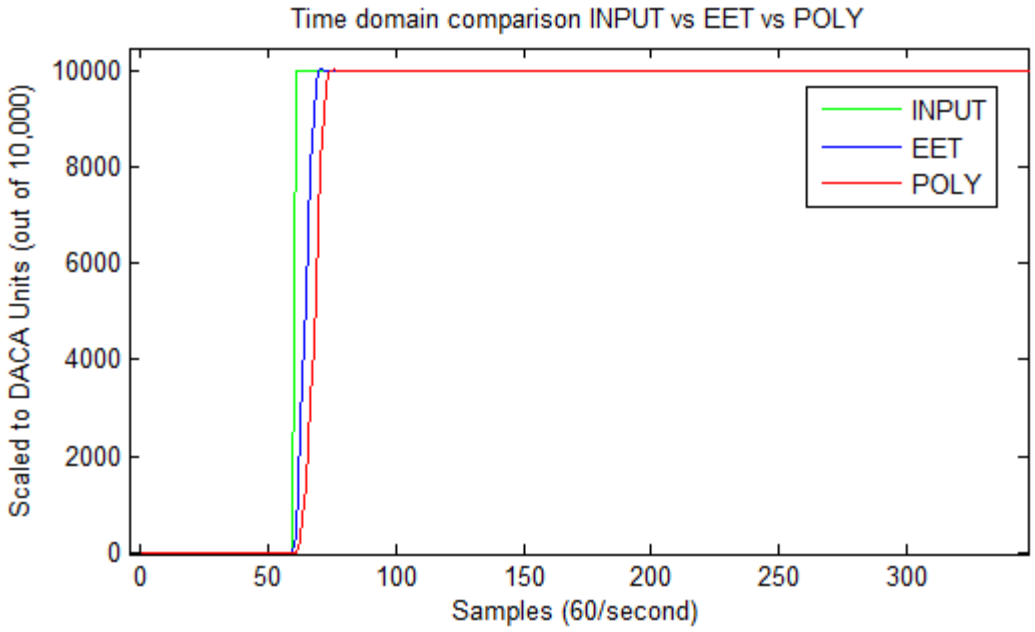

Figure 23. Time Domain Response for Input Signal, Linear Displacement of Actuator Carriage and Output Signal Captured by Polygraph to Step Input for Cardiovascular Channel

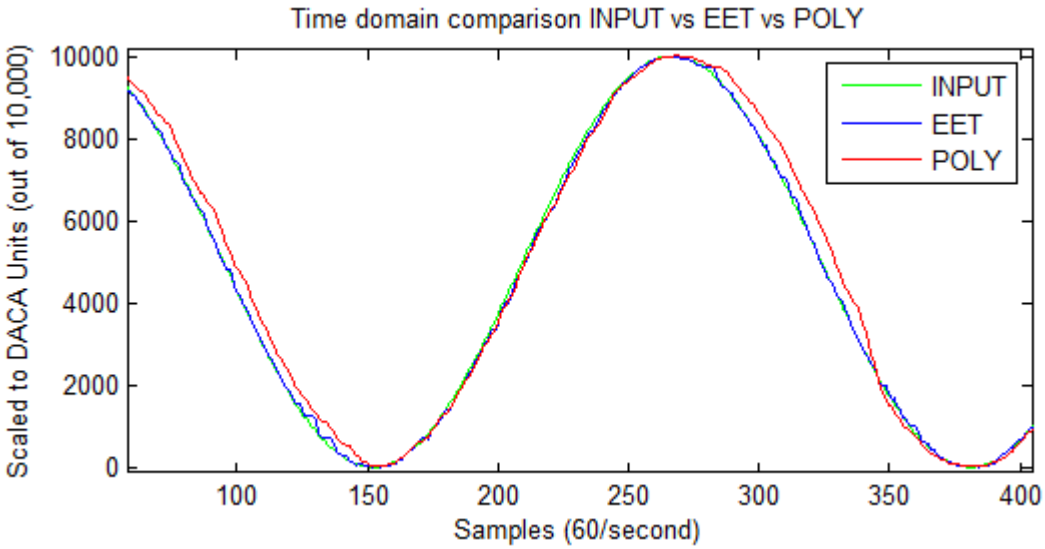

Figure 24. Scaled Time Domain Response for Input Signal, Linear Displacement of Actuator Carriage and Output Signal Captured by Polygraph to Sinusoid Input for Cardiovascular Channel

For each electromechanical channel, and for each of the three inputs to the system, a second-, third- and fourth-order system transfer function model with no initial transport delay

was estimated using MATLAB's system identification tools for both $G_1(s)$ and $G_2(s)$. To determine which transfer functions are the best models for $G_1(s)$ and $G_2(s)$, time response comparisons between transfer function model outputs and measured outputs captured by the potentiometer and the polygraph were performed and evaluated. After processing the time response comparison data between the model output and the measured output, transfer functions whose model outputs produced the least amount of absolute error relative to the measured outputs captured by the potentiometer and polygraph were chosen for the final transfer function models, $G_1(s)$ and $G_2(s)$, of the system. Transfer functions, bode diagrams of the transfer functions and simulation results can be found in the following sections.

5.2.1 Transfer Functions for Respiratory Subsystem

After simulation results were processed, the following transfer functions were chosen to model the respiratory channel on the EET and be considered in compensator design for the respiratory channel:

$$G_1(s) = \frac{16.65s^2 + 121.8s + 244.2}{s^3 + 24.95s^2 + 128.5s + 245.5} \tag{19}$$

$$G_2(s) = \frac{32.81s^2 + 285.4s + 1454}{s^3 + 34.85s^2 + 266.6s + 1454} \tag{20}$$

The dynamics of the system along with simulation results favored a third-order transfer function for both $G_1(s)$ and $G_2(s)$. Figures 25 and 26 display Bode diagrams of the transfer functions $G_1(s)$ and $G_2(s)$ of the respiratory channel, respectively. The transfer functions chosen for $G_1(s)$ and $G_2(s)$ most accurately model the magnitude and phase characteristics of the respiratory subsystem.

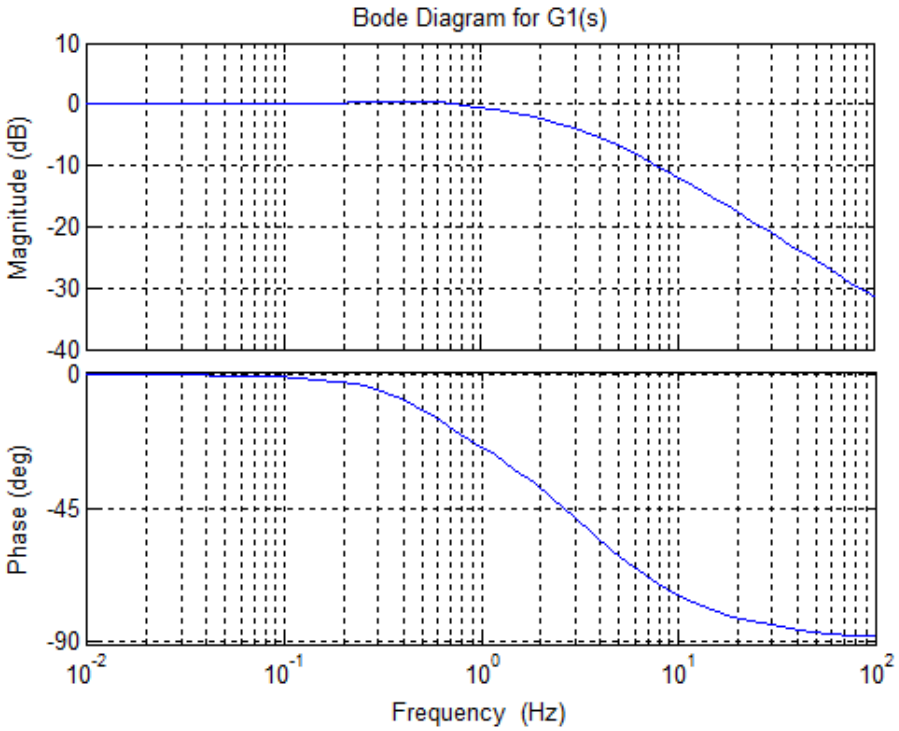

Figure 25. Bode Diagram of $G_1(s)$ of Respiratory Channel

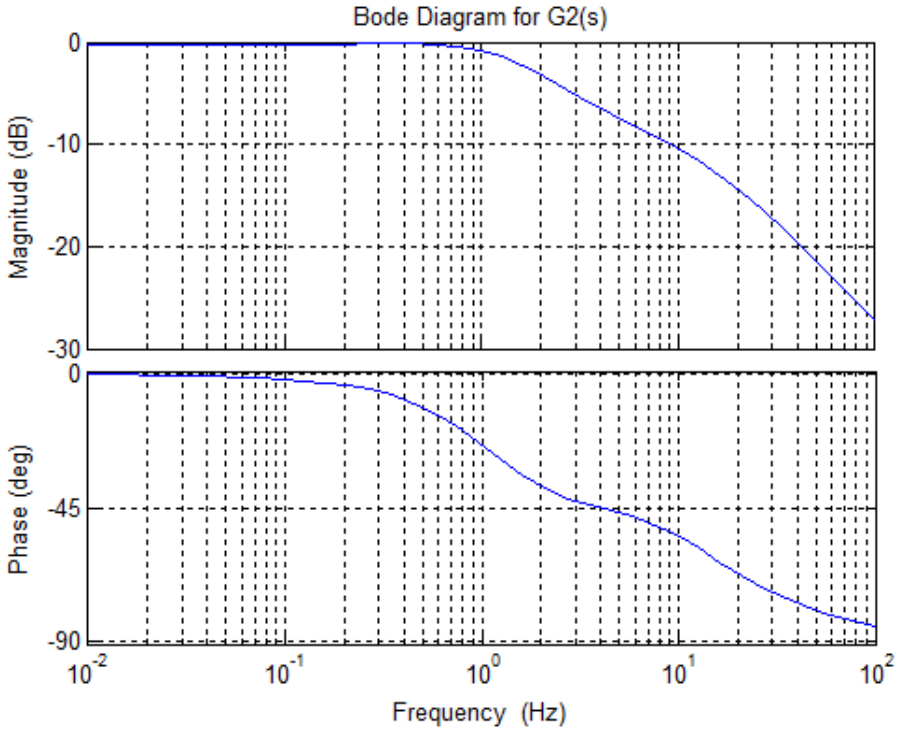

Figure 26. Bode Diagram of $G_2(s)$ of Respiratory Channel

The complete respiratory channel transfer function $G(s)$ can now be defined as follows:

$$G(s) = G_1(s) * G_2(s) \tag{21}$$

$$= \frac{454.9s^4 + 1.705e04s^3 + 1.529e05s^2 + 5.37e05s + 6.63e05}{s^6 + 112.8s^5 + 3311s^4 + 3.912e04s^3 + 2.198e05s^2 + 6.08e05 + 6.962e05}$$

Figure 27 displays a bode diagram of the full subsystem transfer function $G(s)$.

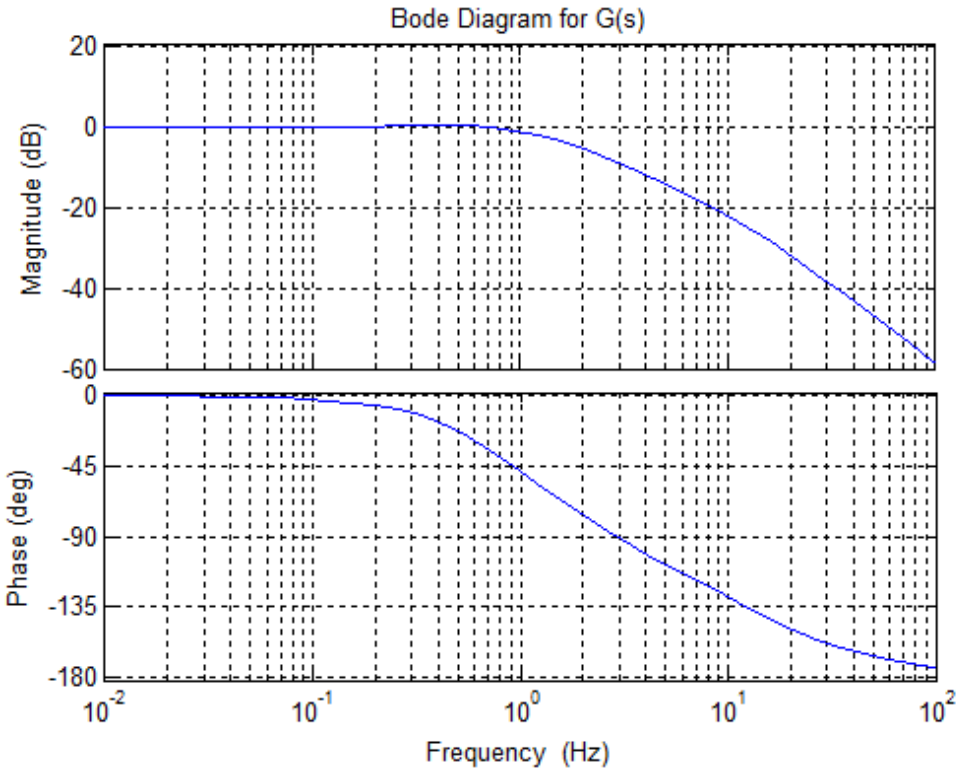

Figure 27. Bode Diagram of G(s) of Respiratory Channel

Now, a time response comparison of the newly defined $G(s)$ model to measured data is necessary to validate $G(s)$. A physiological signal recording was played on the EET and captured by the polygraph. Figure 28 demonstrates the comparison between simulated model

output data and the measured output data. As verified by Figure 28, the transfer function model output closely resembles the measured output.

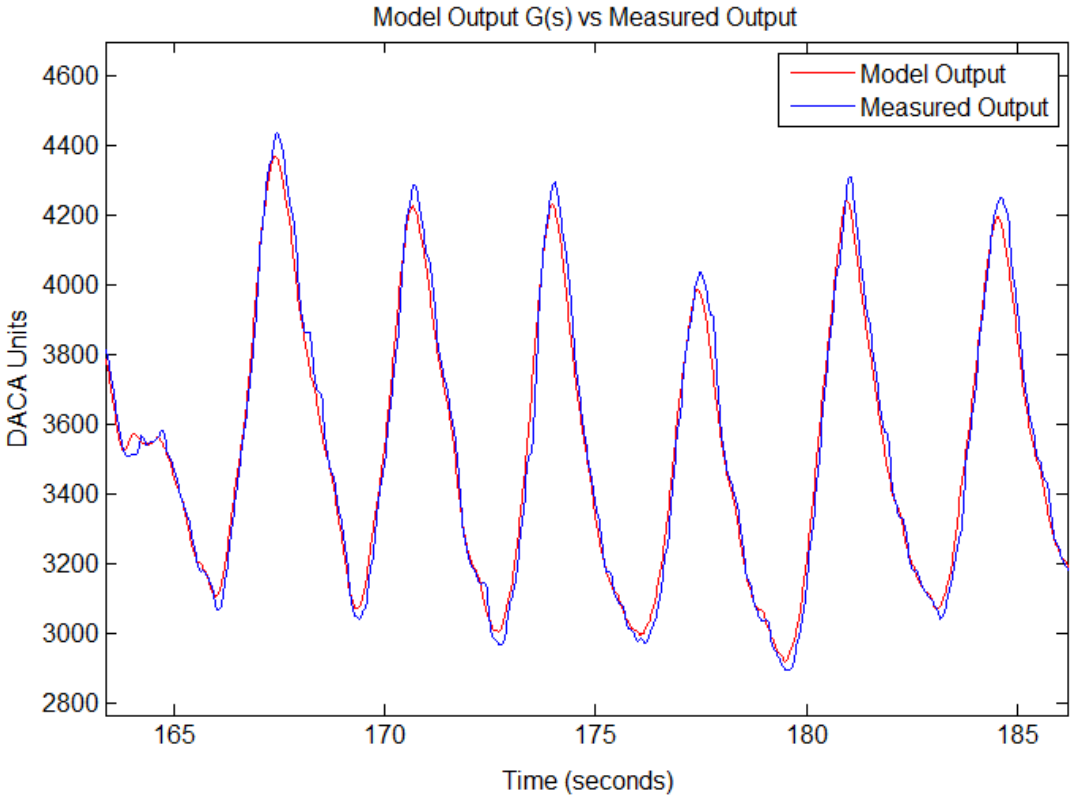

Figure 28. Partial Recording of Comparison between Model Output and Measured Output for Respiratory Channel

5.2.2 Transfer Functions for Cardiovascular Subsystem

Subsequent to simulation results and following the same procedures as the respiratory subsystem, the following transfer functions were chosen to model the respiratory channel on the EET and be considered in compensator design for the cardiovascular channel:

$$G_1(s) = \frac{23.42s^2 + 319.6s + 549.1}{s^3 + 33.70s^2 + 358.6s + 544.2} \quad (22)$$

$$G_2(s) = \frac{32.56s^2 + 803.7s + 4.456e04}{s^3 + 69.81s^2 + 3092s + 4.836e04} \quad (23)$$

The dynamics of the cardiovascular channel closely resemble that of the respiratory channel. Third-order transfer functions were also chosen for $G_1(s)$ and $G_2(s)$ of the cardiovascular channel because of simulation results and the dynamic properties of the system. Figures 29 and 30 display Bode diagrams of the transfer functions $G_1(s)$ and $G_2(s)$ of the cardiovascular channel, respectively.

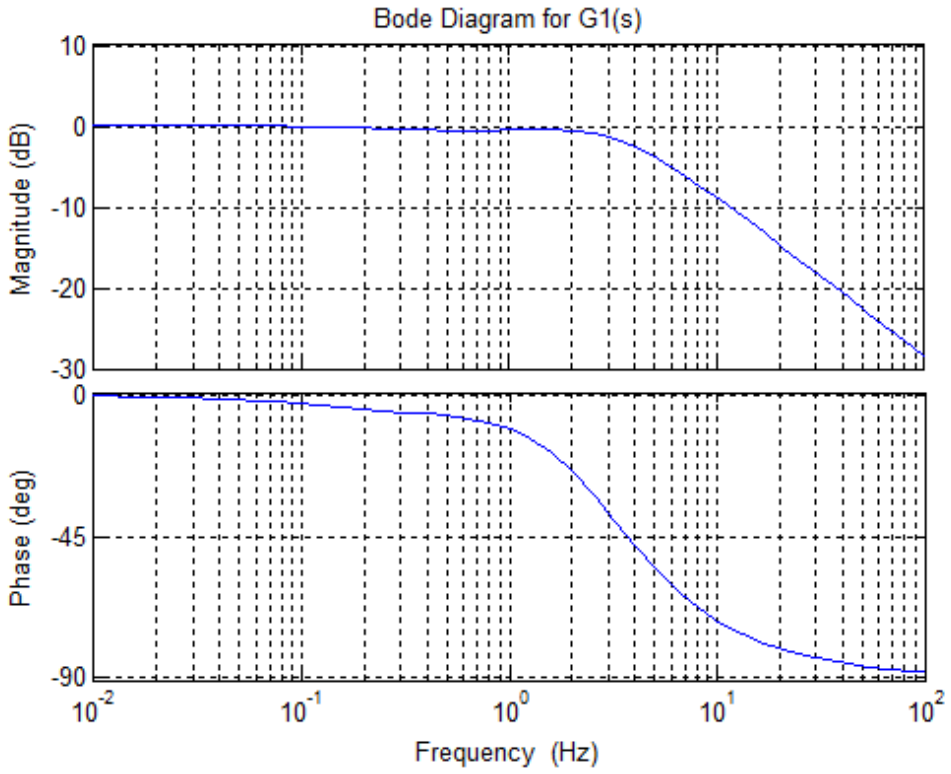

Figure 29. Bode Diagram of $G_1(s)$ of Cardiovascular Channel

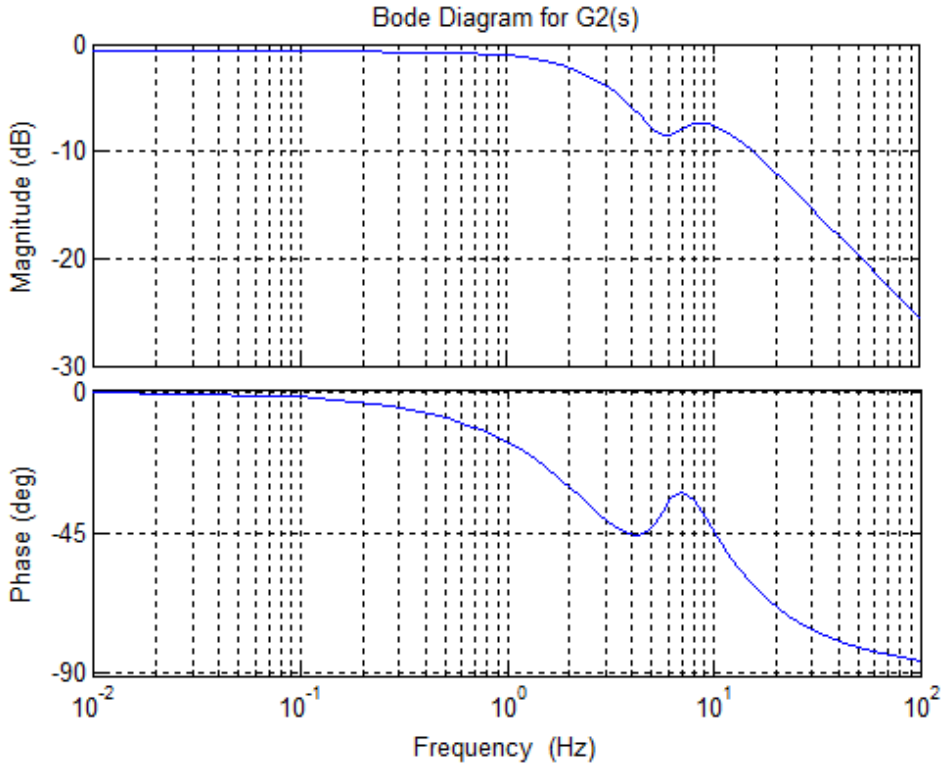

Figure 30. Bode Diagram of $G_2(s)$ of Cardiovascular Channel

The complete cardiovascular channel transfer function $G(s)$ can now be defined as follows:

$$G(s) = G_1(s) * G_2(s) \tag{24}$$

$$= \frac{762.6s^4 + 2.923e04s^3 + 1.318e06s^2 + 1.468e07s + 2.447e07}{s^6 + 103.5s^5 + 5803s^4 + 1.781e05s^3 + 2.777e06s^2 + 1.902e07 + 2.632e07}$$

Figure 31 displays a bode diagram of the full subsystem transfer function $G(s)$.

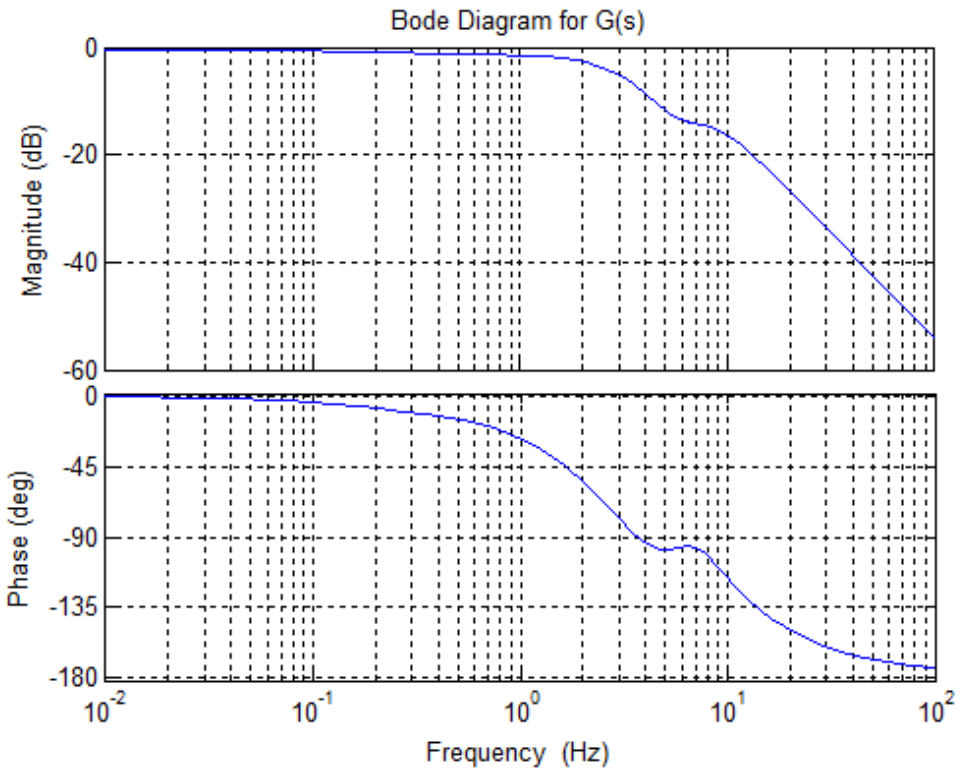

Figure 31. Bode Diagram of G(s) of Cardiovascular Channel

It can be observed that while the Bode diagram of the respiratory subsystem transfer function $G(s)$ is similar to the Bode diagram of the cardiovascular channel subsystem transfer function $G(s)$, there are a few important differences. More specifically, the slopes of the plots of the magnitude and phase angle for frequencies higher than 1 Hz differ. At a frequency of 1 Hz, the magnitude of both the respiratory subsystem transfer function and the cardiovascular subsystem transfer function is -1 dB. At relevant frequencies of 2 and 3 Hz, the magnitude of the transfer function for the respiratory subsystem is roughly twice as small as the magnitude of the transfer function for the cardiovascular subsystem. Although the screw lead on the respiratory channel actuators is approximately twice as large as the screw lead on the cardiovascular channel actuator and has a negligible load, this does not compensate for the fact that the linear displacement of the respiratory channel actuator is 50mm while the linear displacement of the

cardiovascular channel actuator is only 5mm. This gives some understanding of the magnitude and phase characteristics between the two transfer functions.

Now, a time response comparison of $G(s)$ to measured data is necessary to validate $G(s)$ for the cardiovascular channel. A previously recorded physiological signal was played on the EET and captured by the polygraph. Figure 32 demonstrates the comparison between simulated model output data and the measured output data. As verified by Figure 32, the transfer function model output closely resembles the measured output.

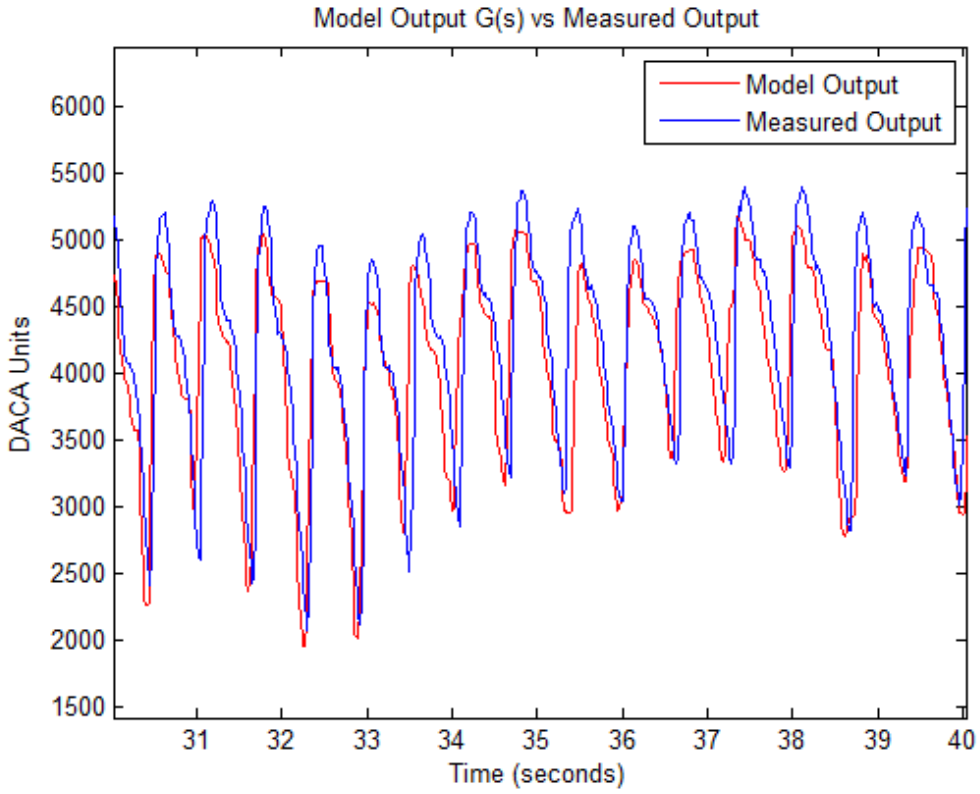

Figure 32. Partial Recording of Comparison between Model Output and Measured Output for Cardiovascular Channel

5.3 Compensator Design

The transfer functions for all electromechanical channels have now been defined; therefore, the compensator component $G_C(s)$ can be designed. Typically, a Phase-Lead, Phase-Lag or Phase-Lead-Lag compensator will be introduced to the system to alter the system in such a way to produce a desirable system response [22]. However, since each channel is independently modeled with one transfer function, it can simply be inverted to produce the desirable system response. Moreover, by introducing the inverse of each subsystem transfer function to the input of the system, the output signal captured by the polygraph should be identical to the input file played on the EET.

5.3.1 Respiratory Subsystem Compensator

The following compensator $G_C(s)$ was defined by taking the inverse of the respiratory subsystem transfer function $G(s)$. This compensator will be introduced to the input of the system as shown in Figure 18.

$$G_C(s) = G(s)^{-1} \tag{25}$$

$$= \frac{s^6 + 112.8s^5 + 3311s^4 + 3.912e04s^3 + 2.198e05s^2 + 6.08e05s + 6.962e05}{454.9s^4 + 1.705e04s^3 + 1.529e05s^2 + 5.37e05s + 6.63e05}$$

Figure 33 displays a Bode diagram of $G_C(s)$ for the respiratory channel. This figure also displays a Bode diagram $G(s)$ in the same window to give some perspective of the contrasting magnitude and phase characteristics of $G(s)$ and $G_C(s)$ for the respiratory channel.

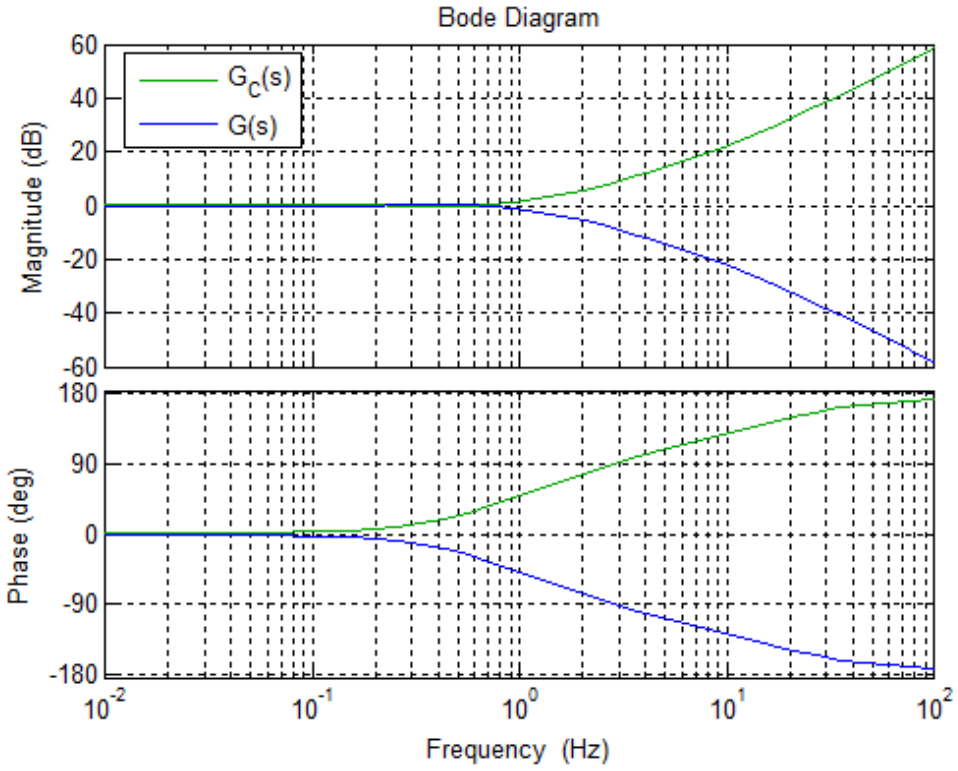

Figure 33. Bode Diagram of $G_C(s)$ Compared to G(s) for the Respiratory Subsystem

5.3.2 Cardiovascular Subsystem Compensator

The following compensator $G_C(s)$ to be introduced to the input of the cardiovascular subsystem was conceived in an identical fashion as for the respiratory subsystem – by taking the inverse of the cardiovascular subsystem transfer function $G(s)$.

$$G_C(s) = G(s)^{-1} \tag{26}$$

$$= \frac{s^6 + 103.5s^5 + 5803s^4 + 1.781e05s^3 + 2.777e06s^2 + 1.902e07s + 2.632e07}{762.6s^4 + 2.923e04s^3 + 1.318e06s^2 + 1.468e07s + 2.447e07}$$

Figure 34 displays a Bode diagram of $G_C(s)$ for the cardiovascular channel. This figure also displays a Bode diagram $G(s)$ in the same window to give some perspective of the contrasting magnitude and phase characteristics of $G(s)$ and $G_C(s)$ of the cardiovascular subsystem.

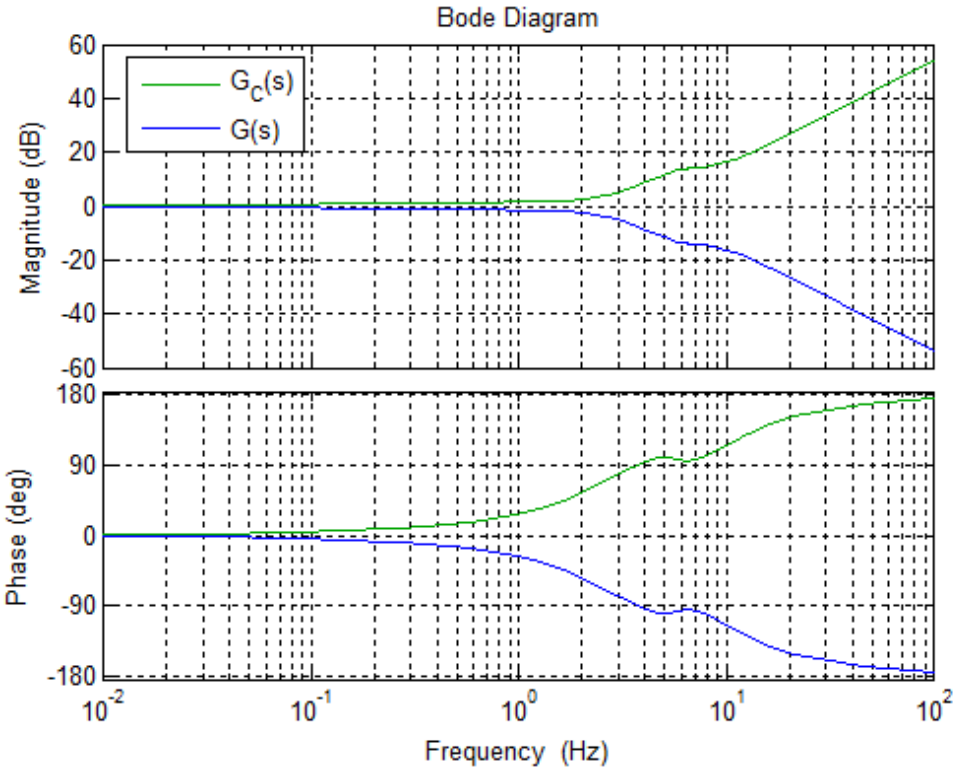

Figure 34. Bode Diagram for $G_C(s)$ Compared to G(s) for the Cardiovascular Subsystem

Now that $G(s)$and $G_C(s)$ for each electromechanical subsystem are defined, $G_C(s)$ can be implemented into the input of the system to achieve the desired system response. The following chapter will cover implementation details and measured output results after introducing the compensator to the system.

CHAPTER 6

COMPENSATOR IMPLEMENTATION AND RESULTS

The compensator designed in Chapter 5 will be cascaded into the system after the input as shown in Figure 18. Rather than compute a compensated input in real time, the implementation of the compensator will be done by preprocessing the inputs to the respiratory and cardiovascular channels. This chapter will cover compensator implementation details and testing results of the EET replicating physiological signals with a compensated input.

6.1 Continuous-Time to Discrete-Time Transfer Function Model Conversion

The transfer functions defined in Chapter 5 are continuous-time transfer function models. These continuous-time transfer functions must be realized as discrete-time transfer functions before introducing them to the digital system. To accomplish this, $G_C(s)$ must be converted to $G_C(z)$. In other words, the continuous-time transfer function in the s-domain must be discretized to a discrete-time transfer function in the z-domain.

In its current state, the compensators for both electromechanical subsystems have two more zeroes than poles. Since transfer functions of this order are not typically found in real systems, this is considered an improper transfer function by MATLAB. Before any simulation or analysis using $G_C(s)$ can be done in MATLAB, it must be of a proper form. In order to satisfy the requirements of MATLAB, two more poles must be added to the transfer function. These poles must be strategically located so they do not affect the frequency characteristics of the

system in the frequency range of interest. This will be implemented to both transfer functions by adding two poles and multiplying by a gain as follows:

$$G_C(s) = G_C(s) * \frac{10000 * 10000}{(s + 10000)(s + 10000)} \tag{27}$$

The following two equations display the new subsystem transfer functions with added poles and a compensated gain for the respiratory and cardiovascular channel, respectively.

$$G_{C(resp)}(s) \tag{28}$$

$$= \frac{1e10s^6 + 1.128e12s^5 + 3.311e13s^4 + 3.912e14s^3 + 2.198e15s^2 + 6.08e15s + 6.962e15}{454.9s^6 + 9.1e07s^5 + 4.552e12s^4 + 1.705e14s^3 + 1.529e15s^2 + 5.37e15s + 6.63e15}$$

$$G_{C(cardio)}(s) \tag{29}$$

$$= \frac{1e10s^6 + 1.035e12s^5 + 5.8e13s^4 + 1.781e15s^3 + 2.777e16s^2 + 1.9e17s + 2.632e17}{762.6s^6 + 1.525e08s^5 + 7.63e12s^4 + 2.926e14s^3 + 1.32e16s^2 + 1.47e17s + 2.447e17}$$

To determine the effect that the additional poles and the compensated gain has on the frequency characteristics of $G_C(s)$, a bode diagram of $G_C(s)$ for the respiratory and cardiovascular channel before and after added poles is shown in Figure 35 and Figure 36.

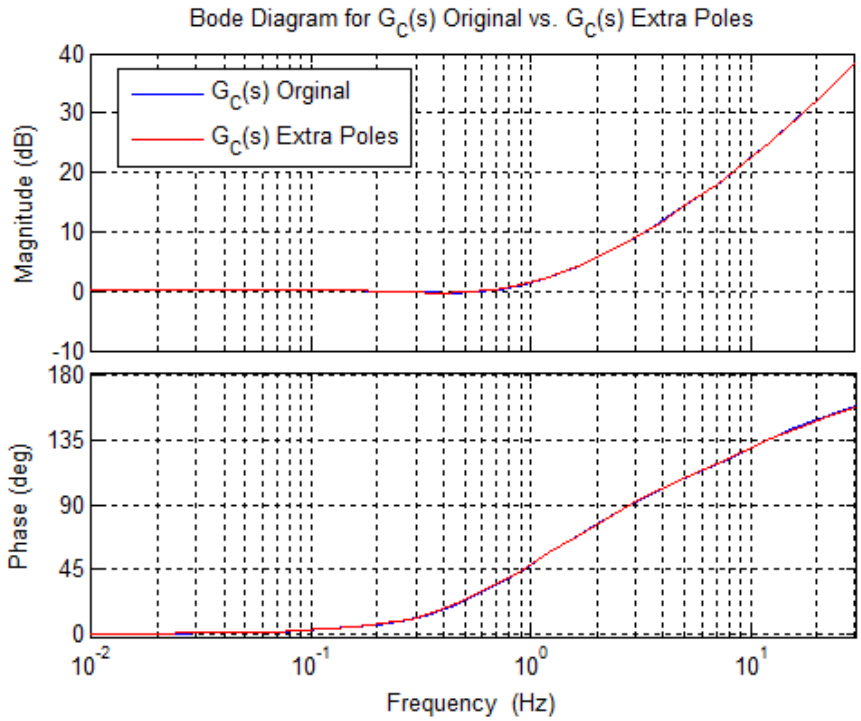

Figure 35. Bode Diagram of Original $G_C(s)$ vs. Proper Form $G_C(s)$ for Respiratory Channel

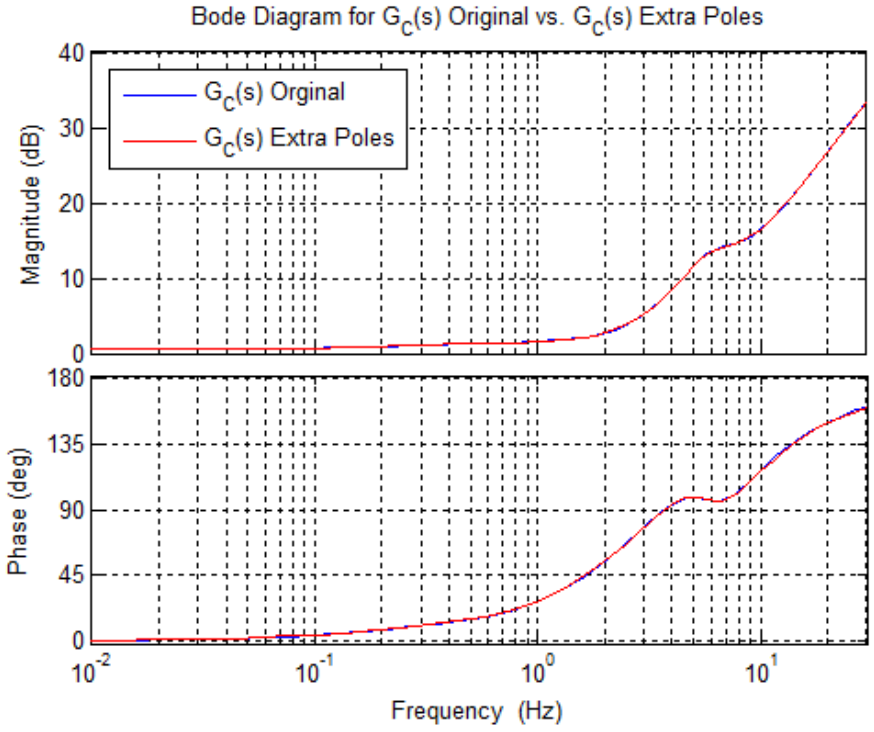

Figure 36. Bode Diagram of Original $G_C(s)$ vs. Proper Form $G_C(s)$ for Cardiovascular Channel

The bode diagrams in Figures 35 and 36 reveal that the frequency responses of the original $G_C(s)$ and the proper form of $G_C(s)$ are essentially identical up to a high frequency (30 Hz). Now that $G_C(s)$ is in a proper form for MATLAB to handle, and the frequency characteristics have been deemed satisfactory, $G_C(s)$ can be discretized to a discrete-time transfer function. $G_C(s)$ was discretized in MATLAB using a first-order hold method on the inputs and a sample time of 1/60 seconds. This is the sample time of all input files in DACA_ASCII format. The following two transfer functions were realized as discrete-time transfer functions for the respiratory and cardiovascular channels:

$$G_{C(resp)}(z) \tag{30}$$

$$= \frac{10.38z^6 - 45.72z^5 + 80.31z^4 - 70.3z + 30.64z^2 - 5.319z - 1.279e-11}{z^6 - 3.464z^5 + 4.468z^4 - 2.539z^3 + 0.5354z^2 + 3.101e-17z + 3.659e-34}$$

$$G_{C(cardio)}(z) \tag{31}$$

$$= \frac{7.005z^6 - 27.64z^5 + 44.42z^4 - 36.57z^3 + 15.49z^2 - 2.706z - 2.628e-16}{z^6 - 3.152z^5 + 3.896z^4 - 2.271z^3 + 0.5279z^2 - 2.437e-17z - 1.029e-34}$$

Figures 37 and 38 displays bode diagrams of $G_C(z)$ compared to $G_C(s)$ for the respiratory and cardiovascular channels. This gives some insight into the spectral characteristics of the discrete-time realization of the system transfer functions $G_C(s)$ for both electromechanical subsystems.

The Bode diagrams reveal that the discrete-time transfer functions become distorted relative to the continuous-time transfer functions as the frequency approaches the Nyquist frequency. Although there are some slight discrepancies in the Bode diagrams of the continuous-time transfer function $G_C(s)$ and the discrete-time transfer function $G_C(z)$, they are almost identical at the frequencies required of the EET. From Table 1, the maximum actuation rate for

the respiratory channel is 0.5 Hz while the maximum actuation rate for the cardiovascular channel is 3.333 Hz. At these actuation rate limits, the frequency characteristics of $G_C(s)$ and $G_C(z)$ are nearly identical for both channels. The only exception is a difference in phase shift in the cardiovascular channel at frequencies above 1Hz. Test data will confirm that this slight variation is phase shift has a negligible effect on the outcome of the system.

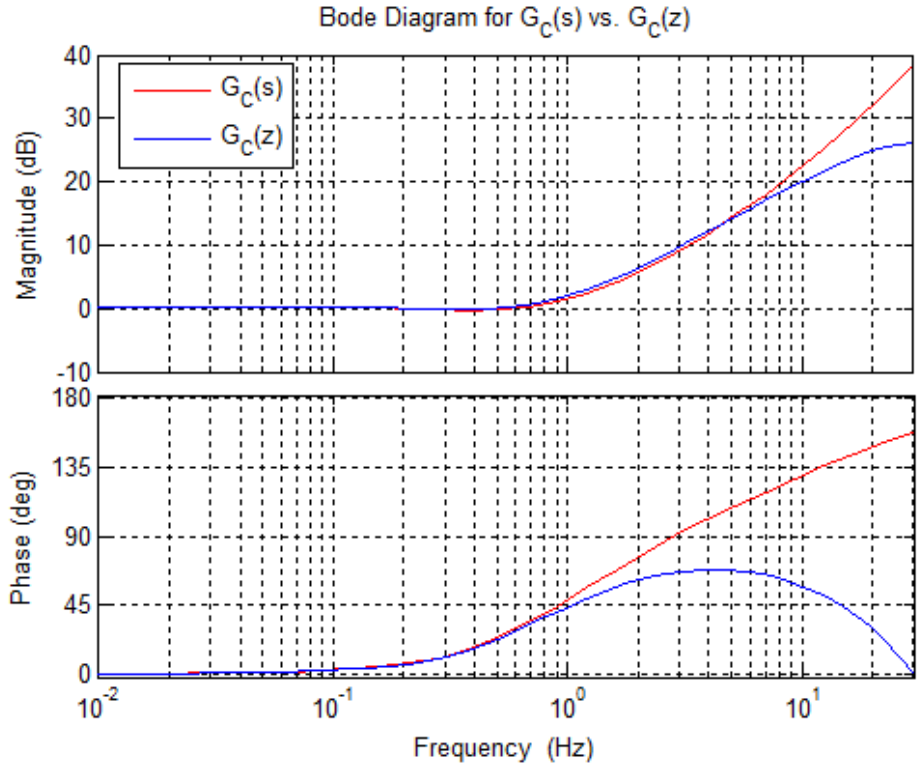

Figure 37. Respiratory Channel $G_C(z)$

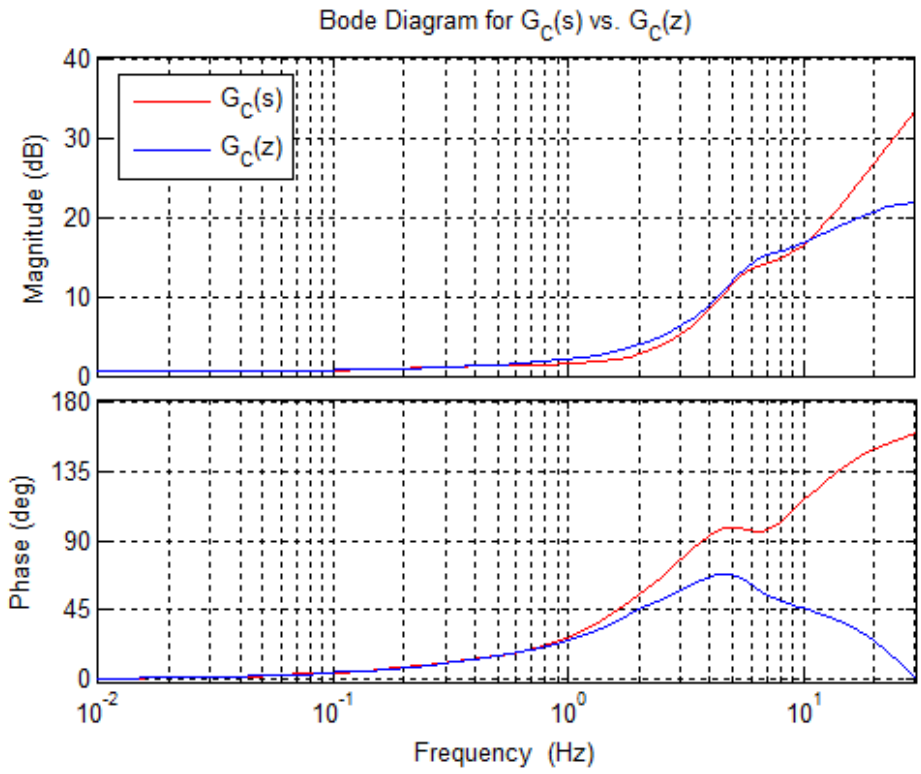

Figure 38. Cardiovascular Channel $G_C(z)$

6.2 Preprocessing Inputs to the EET

Compensator implementation will involve preprocessing the input to the system. Rather than process the inputs in real time via Visual Studio, the inputs will be preprocessed using MATLAB before being inputted into the system. The inputs were preprocessed by simulating the time response of the discrete-time transfer function to each subsystem's input. The output from this simulation will serve as the input signal to the EET. The signals were then renormalized to a 0-10,000 DACA unit scale. This will allow the EET to reproduce the signals without a data range issue while allowing the compensated signal to retain its shape. Sections 5.2.1 and 5.2.2 provide details of the compensated inputs and how they will affect the system response for the respiratory and cardiovascular channels.

6.2.1 Input to the Respiratory Channel

Figures 39 and 40 provide a visual comparison of the original respiratory input signal to the compensated respiratory input signal. The input to the respiratory channel was the same physiological signal used during the validation test suite as described in Section 4.3.4.

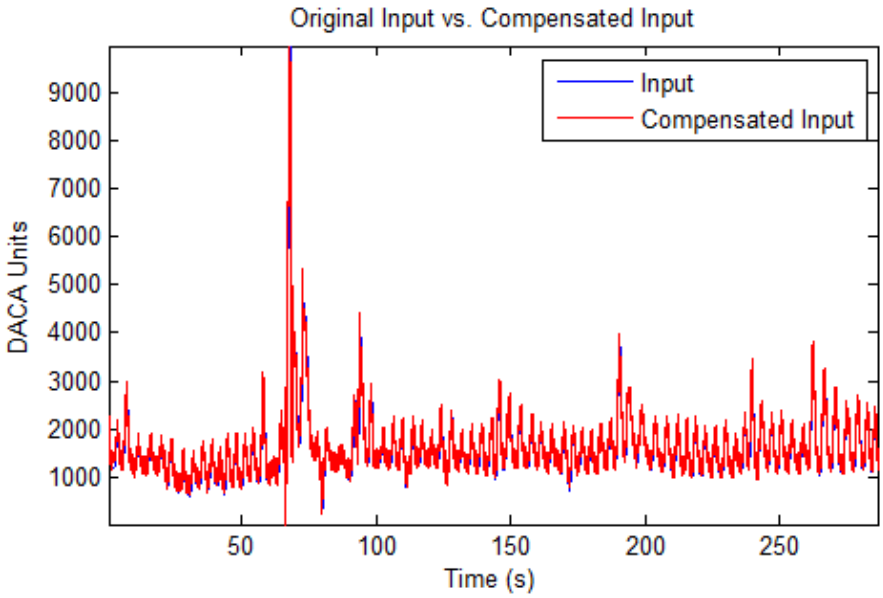

Figure 39. Original Input vs. Compensated Input for Respiratory Channel

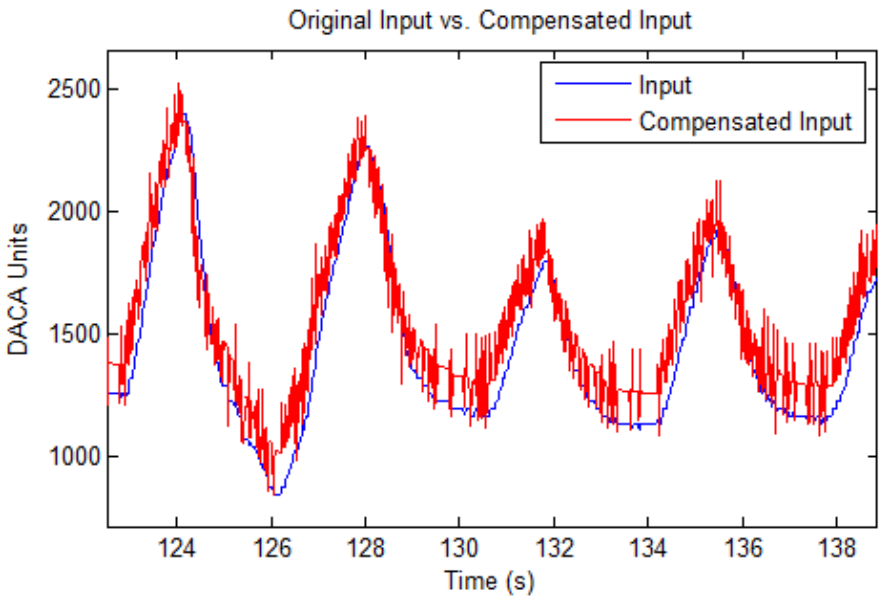

Figure 40. Scaled Original Input vs. Compensated Input for Respiratory Channel

The original input signal has high frequency spectral components convoluted in the low frequency oscillations that make up the respiratory signal. Due to the frequency characteristics of the compensator at high frequencies, the compensated input contains what seems like an inordinate amount of amplification of the high frequency spectral components present in the respiratory signal. However, this is necessary to compensate for the slow dynamics of the system to accurately reproduce the physiological signal associated with the respiratory channel. The test results presented in this chapter will show that this is inconsequential when reproducing signals on the EET.

6.2.2 Input to the Cardiovascular Channel

Figures 41 and 42 provide a visual comparison of the original respiratory input signal to the compensated respiratory input signal. The input to the cardiovascular channel was the same physiological signal used during the validation test suite as described in Section 4.3.4.

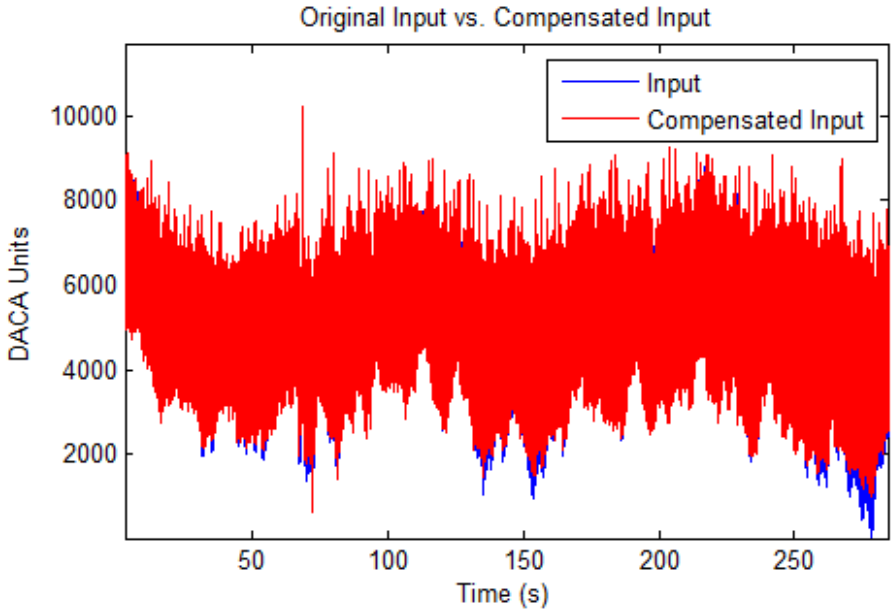

Figure 41. Original Input vs. Compensated Input for Cardiovascular Channel

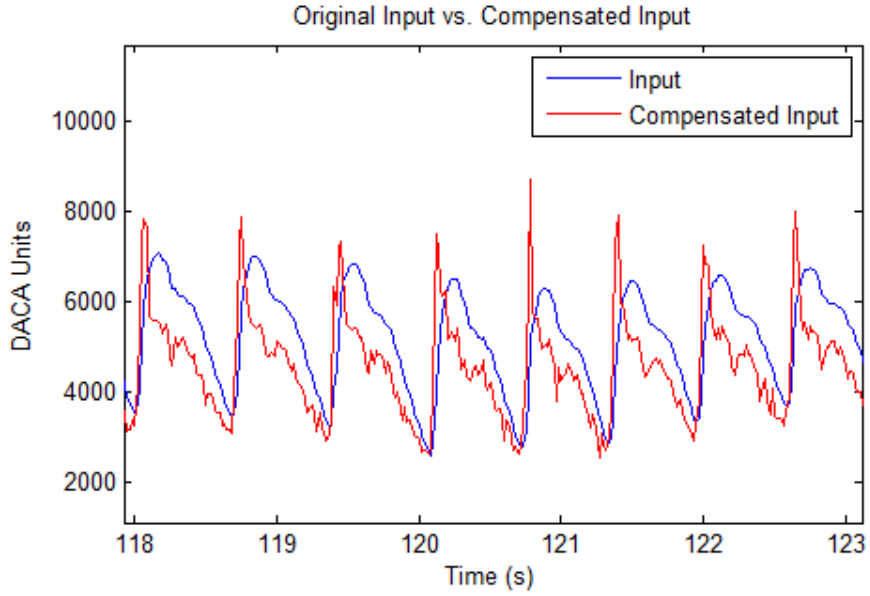

Figure 42. Scaled Original Input vs. Compensated Input for Cardiovascular Channel

As seen with the respiratory channel, the original input signal has high frequency noise convoluted in the low frequency oscillations that make up the respiratory signal. Due to the frequency characteristics of the cardiovascular compensator at high frequencies, the compensated input contains large amplifications of this noise. However, this is necessary to compensate for the slow dynamics of the system to accurately reproduce the physiological signal associated with the respiratory channel. The high frequency components of the cardiovascular input seem to stem more from the natural cardiovascular response, rather than noise obtained during the capture of the cardiovascular activity signal.

6.3 Test Results after Implementation of Compensator

The compensators designed for each subsystem were tested using methods similar to those presented in Chapter 4. A total of 10 separate test signals were captured by the polygraph. Because the human recording used during the validation test suite in Chapter 4 was the same as the human recording that provides the input to the compensator, they can be directly compared to obtain a quantified metric of how well the compensator improved the accuracy of the system. The error metrics E_{REF}, E_{MEAN} and STD_{MEAN} were calculated for the compensator tests and compared to the validation tests from Chapter 4.

6.3.1 Results of Respiratory Channel Compensator and Discussion

Figures 43 and 44 demonstrate the comparison of recorded signals being played back on the EET (original signals) vs. the signals captured from the EET by the polygraph (reproduced signals) for the human recording after the implementation of the compensator for the respiratory subsystem. Also captured in Figures 43 and 44 are the signals captured from the EET by the

polygraph before the compensator was introduced to the system. Table 8 provides the results of the error metrics used to evaluate accuracy and repeatability of reproduction for human recorded signals for the respiratory channel before and after the compensation of the system.

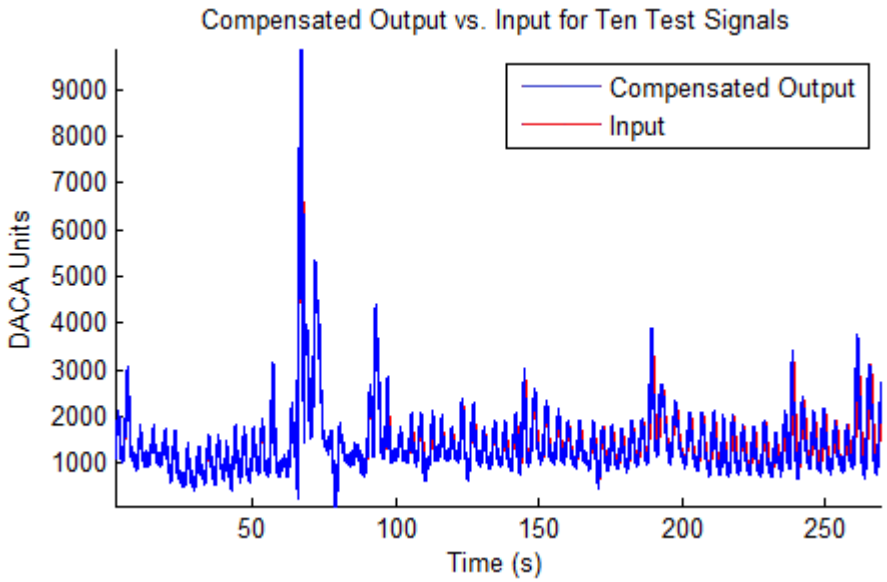

Figure 43. Compensated Output vs. Input for Ten Test Signals on Respiratory Channel

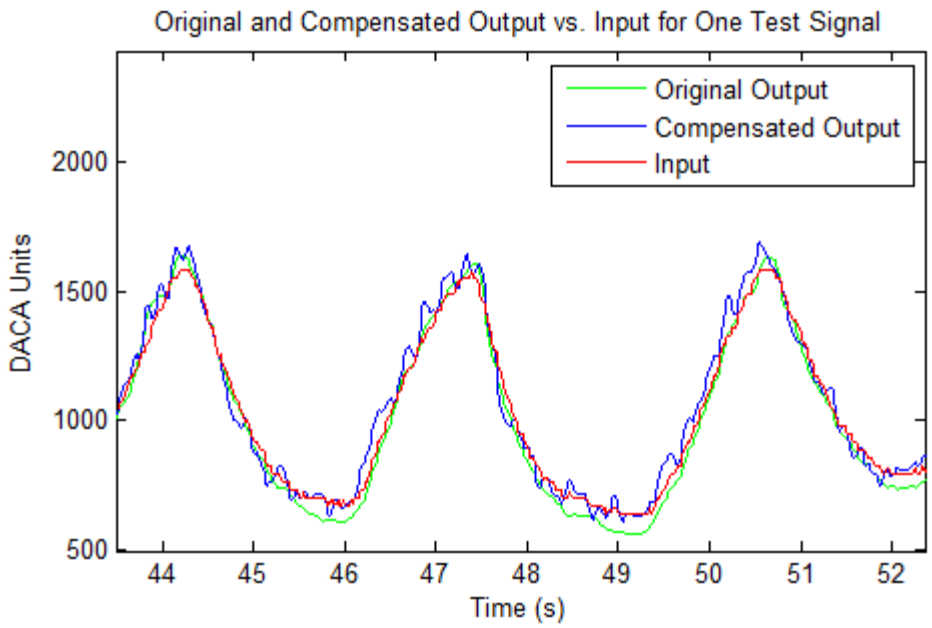

Figure 44. Original and Compensated Output vs. Input for One Test Signal on Respiratory Channel (Scaled)

Table 8. Error Results for Respiratory Channel Compensator

Error Statistic	**Error Measure without Compensation**	**Error Measure with Compensation**
E_{REF}	157.9 (1.58 %)	135.4 (1.35 %)
E_{MEAN}	26.4 (0.26 %)	57.4 (0.57 %)
STD_{MEAN}	159.7 (1.60 %)	90.8 (0.91 %)

The implementation of the compensator in the respiratory subsystem showed an improvement in accuracy (E_{REF}) by 22.5 DACA units, or 14.25%. There was also an improvement in standard deviation (STD_{MEAN}) by 68.9 DACA units, or 43.1%. However, there was a decline in the repeatability of the signal (E_{MEAN}) after compensation by 31 DACA units, or 54%. The compensator introduced to the respiratory channel improved accuracy and standard deviation from the mean signal, but showed a slight decline in repeatability. This could stem

from the amplification of the high frequency noise convoluted into the input signal. The large amplification of the high frequency spectral components convoluted into the respiratory signal lead to a rather noisy output signal as verified in Figure 25. The accuracy of the respiratory system was improved. However, this caused a slight decline in the repeatability of the respiratory subsystem.

6.3.2 Results of Cardiovascular Channel Compensator and Discussion

Figures 45 and 46 demonstrate the comparison of recorded signals being played back on EET (original signals) vs. signals captured from the EET by the polygraph (reproduced signals) for the human recording after the implementation of the compensator for the cardiovascular subsystem. Figures 45 and 46 also demonstrate a comparison of the signals captured from the EET by the polygraph before the compensator was introduced to the system to the signals captured from the EET by the polygraph after the compensator was introduced to the system. Table 9 provides a summary of error representing accuracy and repeatability of reproduction for human recorded signals for the cardiovascular channel before and after the compensator was introduced to the system.

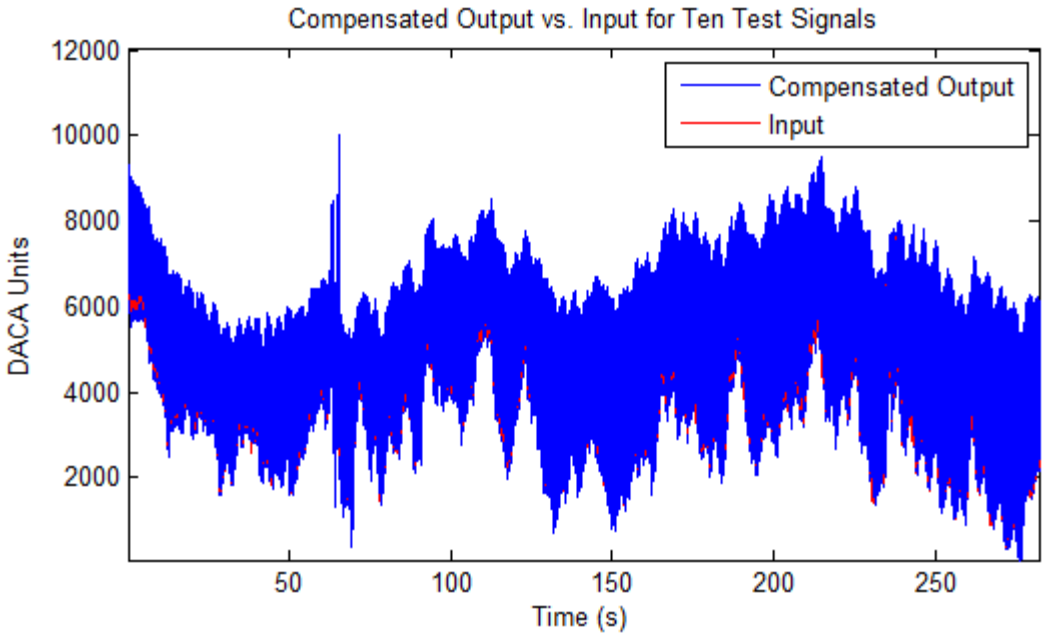

Figure 45. Compensated Output vs. Input for Ten Test Signals on Cardiovascular Channel

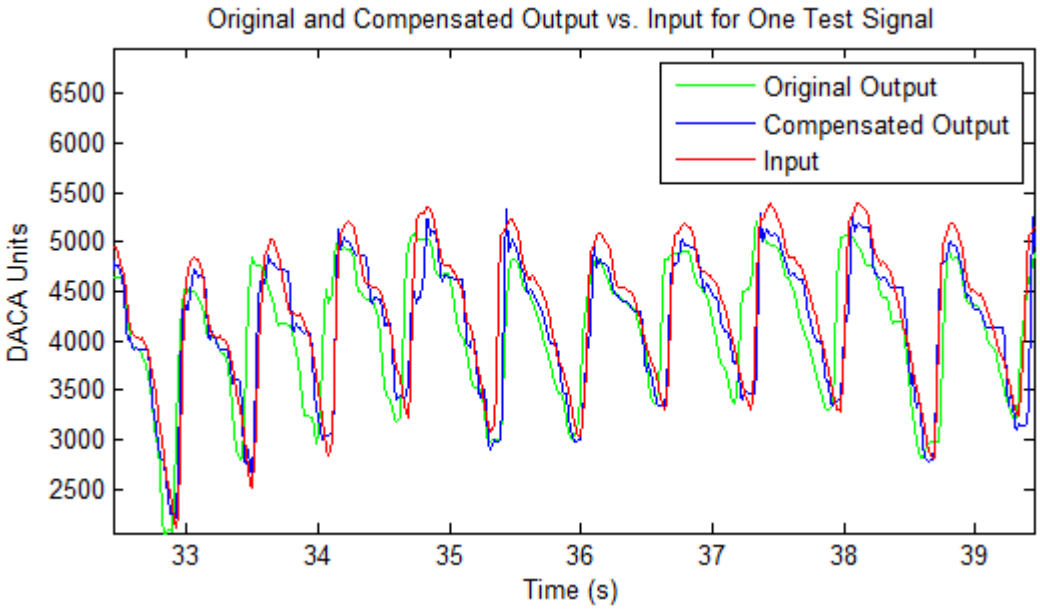

Figure 46. Original and Compensated Output vs. Input for One Test Signal on Cardiovascular Channel (Scaled)

Table 9. Error Results for Cardiovascular Channel Compensator

Error Statistic	**Error Measure without Compensation**	**Error Measure with Compensation**
E_{REF}	209.2 (2.09 %)	191.4 (1.91 %)
E_{MEAN}	91.8 (0.92 %)	89.2 (0.89 %)
STD_{MEAN}	180.1 (1.80 %)	184.7 (1.85 %)

The implementation of the compensator in the cardiovascular subsystem showed a slight improvement in accuracy (E_{REF}) by 17.8 DACA units, or 8.5%. The repeatability (E_{MEAN}) and standard deviation (STD_{MEAN}) of the output signal after compensation was extremely similar to the repeatability and standard deviation of the output signal before compensation. The E_{MEAN} of the output signal after compensation improved by 2.6 DACA units, or 2.8% while the STD_{MEAN} decreased by 4.6 DACA units, or 2.5%. Although the compensator introduced to the cardiovascular channel showed almost no change in the repeatability of the signal, there was an improvement in the absolute error between the output and input signals.

CHAPTER 7

FUTURE WORK AND CONCLUSION

There are a number of future work and research opportunities that are associated with the ability to accurately and repeatedly reproduce physiological and other known signals through electrical and electromechanical means that have yet to be explored. The final chapter of this thesis will take a look at some of those applications and provide a needed conclusion.

7.1 Future Work and Research Opportunities

One area of future work on the EET would involve expanding the validation test suite, as described in Chapter 4, to include accuracy and repeatability tests among several EET prototypes as well as several different polygraph instruments. This is important in assuring there are no major differences between EET prototypes and that the reproduction of physiological signals is accurate and repeatable on several different polygraph instruments. This could be expanded from a modeling standpoint to define transfer functions for several different polygraph instruments. If transfer characteristics vary drastically among different polygraph instruments, a unique compensator can be implemented into the system to assure the most accurate reproduction of physiological signals for each polygraph instrument.

Another area of future work on the EET would involve the expansion of the number of channels associated with the EET. As presented in this thesis, the EET is currently able to electrically and electromechanically reproduce physiological signals associated with respiratory

activity (thoracic and abdominal), cardiovascular activity, and GSR. However, there are polygraph instruments that have the capability to measure several other physiological signals to use in the detection of deception. One example is the LX5000 polygraph instrument [25] from Lafayette Instrument Company. This particular polygraph instrument contains an "activity" sensor with three separate channels (feet, seat, and arms). The EET could reproduce various movement activity signals by controlling solenoid actuators to apply direct actuation to each respective movement activity sensor.

Another research opportunity that is brought about by the ability to electrically and electromechanically reproduce physiological signals is the calibration and periodic testing of various medical devices. For example, an electrocardiogram (EKG) measures the electrical impulses that the heart generates as it is beating [26]. A device similar to the EET presented in this thesis could be used to reproduce similar electrical impulses to calibrate and test EKGs. Many different test signals could be used to detect how a particular EKG would respond to several different heart beat abnormalities especially of those following a heart attack. The ability to accurately and repeatedly reproduce physiological signals of this caliber could not only be beneficial in calibrating various medical devices but also in training doctors and nurses to detect abnormalities in the physiological activity in patients.

7.2 Conclusion

In summary, an Electronic and Electromechanical Tester (EET) designed for the testing of physiological sensors typically associated with polygraph instruments has been presented. While the process of electrically and electromechanically reproducing known signals is not unique in itself, the EET is designed to specifically reproduce physiological signals with the

intention of testing and calibrating polygraph instruments. The EET was implemented to provide direct actuation to the polygraph sensors that are placed on humans during data acquisition and in this way simulate physical manifestations of physiological processes rather their electrical equivalents.

Testing of the EET demonstrated sufficiently high accuracy and repeatability of the reproduced signals, supporting its use for validation of polygraph equipment. Furthermore, accurate transfer function models of the electromechanical channels of this system were defined. Using the information from these transfer function models, a compensator was designed and implemented into the system. The compensator was used to neutralize the transfer characteristics of the EET and polygraph during reproduction of physiological signals with the end goal of more accurately reproducing physiological signals. These test results showed that the implementation of the compensator improved upon the accuracy of reproduction of physiological signals. Overall, it was experimentally determined that the EET was able to successfully electrically and electromechanically reproduce physiological signals originating from the human body.

REFERENCES

[1] K. Alder, The Lie Detectors: The History of an American Obsession. Simon and Schuster, 2007.

[2] Wikipedia contributors, "Polygraph," Wikipedia, the free encyclopedia. Wikimedia Foundation, Inc., 02-Aug-2012.

[3] L. Saxe, D. Dougherty, and T. Cross, "The validity of polygraph testing: Scientific analysis and public controversy," American Psychologist, vol. 40, no. 3, pp. 355–366, 1985.

[4] W. G. Iacono, "Forensic lie detection : Procedures without scientific basis," Journal of forensic psychology practice, vol. 1, no. 1, pp. 75–86.

[5] L. A. Geddes, "The truth shall set you free [development of the polygraph]," IEEE Engineering in Medicine and Biology Magazine, vol. 21, no. 3, pp. 97 –100, Jun. 2002.

[6] D. C. Fowles, M. J. Christie, R. Edelberg, W. W. Grings, D. T. Lykken, and P. H. Venables, "Publication Recommendations for Electrodermal Measurements," Psychophysiology, vol. 18, no. 3, pp. 232–239, 1981.

[7] P. Zhu, L. Chen, "Design of Automated Oscillometric Electronic Sphygmomanometer Based on MSP430F449," 2010 International Conference on Future Information Technology and Management Engineering, vol. 1, pp. 463-466, Oct. 2010

[8] "Arduino Mega 2560 – Arduino SA." [Online]. Available: http://arduino.cc/en/Main/ArduinoBoardMega2560. [Accessed: 13-Oct-2013].

[9] "ATmega16U2 - Atmel Corporation." [Online]. Available: http://www.atmel.com/devices/atmega16u2.aspx. [Accessed: 13-Oct-2013].

[10] "ATmega2560 - Atmel Corporation." [Online]. Available: http://www.atmel.com/devices/atmega2560.aspx. [Accessed: 13-Oct-2013].

[11] Maxim Integrated, "Low-Power, Slew-Rate-Limited RS-485/RS-422 Transceivers," MAX485 datasheet, Sept. 2009.

[12] STMicroelectronics, "Single bilateral switch," 74V1G66 datasheet, Oct. 2008.

[13] W. Boucsein. Electrodermal Activity, 2nd ed. New York, Springer Publishing, 2012.

[14] Texas Instruments, "ULTRALOW NOISE, HIGH PSRR, FAST RF, 100-mA LOW-DROPOUT LINEAR REGULATORS," TPS79147 datasheet, June 2008.

[15] “Acromag.” [Online]. Available: http://www.acromag.com/catalog/746. [Accessed: 16-May-2013].

[16] “Fastech.” [Online]. Available: http://www.fastech.co.kr/bbs/data/product/942952012121709201901.pdf . [Accessed: 16-May-2013].

[17] “Miniature Linear Actuators.” [Online]. Available: http://www.pbclinear.com/ML---Miniature-Linear-Actuators. [Accessed: 13-Aug-2012].

[18] “Pelican.” [Online]. Available: http://www.pelican.com/cases_detail.php?Case=1610. [Accessed: 13-Oct-2013].

[19] “LX4000 Polygraph System | Polygraph from Lafayette Instrument Company.” [Online]. Available: http://www.lafayettepolygraph.com/product_list.asp?subcatid=41. [Accessed: 12-Aug-2012].

[20] M. Tarvainen, A. Koistinen, M. Valkononen-Korhonen, J. Partanen, P. Karjalainen, “Analysis of Galvanic Skin Responses With Principal Components and Clustering Techniques,” IEEE Transactions on Biomedical Engineering, vol. 48, no. 10, pp. 1071-1079, Oct. 2001.

[21] A. B. DuBois, A. W. Brody, D. H. Lewis, and B. F. Burgess, “Oscillation Mechanics of Lungs and Chest in Man,” J Appl Physiol, vol. 8, no. 6, pp. 587–594, May 1956.

[22] R. C. Dorf and R. H. Bishop, *Modern Control Systems*. Upper Saddle River, NJ: Pearson Education, Inc., 2011.

[23] “Spectra Symbol.” [Online]. Available: http://www.spectrasymbol.com/potentiometer/softpot. [Accessed: 13-Oct-2013].

[24] The MathWorks Inc., *MATLAB version 8.1.0.604*. Natick, Massachusetts: 2013.

[25] “LX5000 Polygraph System | Polygraph from Lafayette Instrument Company.” [Online]. Available: http://www.lafayettepolygraph.com/product_list.asp?subcatid=196. [Accessed: 13-Oct-2013].

[26] T. R. F. Fulford-Jones, G. Wei and M. Welsh, “A Portable, Low-Power, Wireless Two-Lead EKG System,” In Proc. International Conference of the IEEE EMBS, 2004, pp. 2141-2144.